

1  
2  
3  
4 **A Temporal Waterline Approach to Mapping Intertidal Areas Using X-band Marine Radar.**

5  
6 Paul S. Bell <sup>a</sup>, Cai O. Bird <sup>b</sup> & Andrew J. Plater <sup>b</sup>  
7  
8  
9

10 <sup>a</sup> National Oceanography Centre, Liverpool, United Kingdom (psb@noc.ac.uk) Corresponding author

11  
12 <sup>b</sup> University of Liverpool, School of Environmental Science, United Kingdom.  
13

14 **Abstract**

15  
16 **Mapping the morphology of intertidal areas is a logistically challenging, time consuming and**  
17  
18 **expensive task due to their large expanse and difficulties associated with access. A technique is**  
19  
20 **presented here that uses standard marine navigational radar operating at X-band frequency. The**  
21  
22 **method uses a series of time-exposure radar images over the course of a two-week tidal cycle to**  
23  
24 **identify the elevation of the wetting and drying transitions at each pixel in the radar images,**  
25  
26 **thereby building up a morphological map of the target intertidal area. This “Temporal Waterline”**  
27  
28 **method is applied to a dataset acquired from Hilbre Island at the mouth of the Dee Estuary, UK,**  
29  
30 **spanning March 2006 to January 2007. The radar gathered data with a radial range of 4 km and**  
31  
32 **the resulting elevation maps describe the intertidal regions of that area. The results are compared**  
33  
34 **with airborne LiDAR data surveyed over the same area and within the radar survey time period.**  
35  
36 **The residual differences show good agreement across large areas of beach and sandbanks, with**  
37  
38 **concentrations of poor estimations around points that are shadowed from the radar or likely to**  
39  
40 **suffer from pooling water. This paper presents the theoretical framework of the method and**  
41  
42 **demonstrates its stability and accuracy. The Temporal Waterline radar method is aimed at**  
43  
44 **providing a useful tool for the monitoring and operational management of coastlines.**  
45  
46  
47  
48  
49

50  
51 **Keywords: remote sensing; marine radar; waterline; intertidal mapping; coastal monitoring.**  
52

53  
54 **1. Introduction**

55  
56 **1.1. The importance of mapping intertidal morphology**  
57  
58  
59  
60  
61  
62  
63  
64  
65

1  
2  
3  
4 Coastal, shallow water environments are important to commercial activities as they are often the  
5  
6 site of ports, harbours and recreational areas which represent high value assets in the provision of  
7  
8 various ecosystem services and are the foundation of many local and national economies. These  
9  
10 shallow water systems are also incredibly dynamic and their morphology is known to change  
11  
12 significantly during high energy storm events, and more gradually during more average conditions.  
13  
14 The nature, extent and timescales of such changes at a variety of intertidal areas around the world  
15  
16 has been well documented (Fisher and Stauble, 1977; Fitzgerald et al., 1994; Morton et al., 1995;  
17  
18 Nicholls and Marston, 1939; Sexton and Moslow, 1981; Stone et al., 1996). Changes in morphology  
19  
20 can compromise navigation channels and inlets in a variety of ways (FitzGerald et al., 2000) and can  
21  
22 have significant financial consequences; the United States spends more than \$100 million annually  
23  
24 on Federal channel maintenance, dredging between 50 and 100 million m<sup>3</sup> of sand (Rosati and Kraus,  
25  
26 2000).  
27  
28  
29

30  
31 At a regional level, strategic ports located in morphologically dynamic areas such as river deltas can  
32  
33 experience significant navigation channel disruption due to sedimentation. An example of this is Port  
34  
35 Harcourt located in the Bonny River estuary which empties into the Niger Delta region, Nigeria. This  
36  
37 Port is a crucial gateway to the oil-producing region, and the complicated system of sandbars and  
38  
39 shoals combined with dynamic bank and shoreline erosion present navigational risks to shipping  
40  
41 operating in the vicinity of the port. Often the series of exposed jetties in the Bonny River estuary  
42  
43 are isolated as the shoreline is eroded (Diop et al., 2014). This area is too large and exposed to  
44  
45 monitor manually with ease and therefore a method of remotely monitoring the health and  
46  
47 morphology of the coastline in dynamic areas such as this could be highly effective. Another  
48  
49 example of a vulnerable area is the mouth of the Amazon River, where sandbanks are known to  
50  
51 encroach upon the critical navigation channels. Sand bank migration rates of up to 250 m/year have  
52  
53 been observed here (Fernandes et al., 2007), causing significant disruption to the operation of the  
54  
55 ports.  
56  
57  
58  
59  
60  
61  
62  
63  
64  
65

1  
2  
3  
4 At a more focussed, local scale the Port of Liverpool in the UK removed an average of 1.86 million  
5  
6 tonnes of dredged sediment annually between 2005-2009. This material was extracted from the  
7  
8 navigation channel and berthing zones, areas which are known to be significantly influenced by  
9  
10 migrating sedimentary bed features (Bailey, 2009). Migration of allochthonous sediment into  
11  
12 estuaries is a prevalent problem in port management, specifically in estuaries where ports are  
13  
14 present. The changing sediment budget combined with climate change-induced rising sea level and  
15  
16 changing bathymetry could result in the "squeezing out" of valuable intertidal habitats that lie  
17  
18 between hard sea defences and the shoreline (De Vriend et al., 2011). Experiments have been  
19  
20 conducted involving the disposal of dredged material at eroding beach sites in order to supply  
21  
22 sediment replacement (van der Wal et al., 2011). Schemes such as this, along with planned and  
23  
24 ongoing large-scale sand-scaping / sand engine operations in the UK and Holland (Stive et al., 2013),  
25  
26 also see Zandmotor (<http://www.dezandmotor.nl/en-GB/>), which seek to change the shape of a  
27  
28 coastline in order to increase the socio-economic potential of the area, would benefit greatly from a  
29  
30 cost effective method of long-term intertidal monitoring. In addition, significant cost savings and  
31  
32 improvements in the efficiency of dredging operations and coastal defence construction may be  
33  
34 made through wide area intertidal surveillance and prediction of large-scale sediment migration.  
35  
36 This paper describes and presents a novel technique for mapping the changes in intertidal coastal  
37  
38 morphology across varying timescales using standard marine radar operating at X-band, providing  
39  
40 much needed situational awareness in intertidal areas and utilising existing port infrastructure,  
41  
42 whilst keeping operational costs to a minimum.  
43  
44  
45  
46  
47

## 48 **1.2. Current methods of surveying intertidal areas**

49  
50  
51  
52 The task of surveying intertidal areas has traditionally been performed using well established survey  
53  
54 methods. When the water level is sufficiently high, shallow draft vessels fitted with echosounders  
55  
56 may be used, and when the water level is low enough to expose the area, survey lines may be  
57  
58 walked by a surveyor equipped with a high accuracy GPS system or driven via a GPS equipped all-  
59  
60  
61  
62  
63  
64  
65

1  
2  
3  
4 terrain vehicle. The use of vessel-based multibeam echo sounder surveys is constrained by expense  
5  
6 and inefficiency of operation over large areas and the limited swath width in shallow waters (Gao,  
7  
8 2009). Airborne LiDAR (Light detection and ranging, Lyzenga (1985)) is a non-imaging technique  
9  
10 using laser pulses to detect the range to the ground at low water or the water surface in wet areas.  
11  
12 More advanced versions can distinguish the signals from the water surface and the secondary  
13  
14 reflection from the sea bed provided water clarity is sufficiently good. In recent years, airborne  
15  
16 LiDAR has become the tool of choice for surveying large intertidal areas and multiple surveys flown  
17  
18 over the same area can be used to accurately monitor changes in bathymetry (Guenther et al.,  
19  
20 2000). Although these techniques have improved significantly in accuracy and applicability over  
21  
22 recent decades, they remain expensive, relatively time consuming and rarely run over the same area  
23  
24 on a routine basis. Consequently, data recorded in dynamic areas quickly becomes obsolete until the  
25  
26 next survey. When used in this manner these methods provide only snapshots of episodic  
27  
28 morphological change over relatively long timescales. In order to compliment these accurate and  
29  
30 focused surveys, a method that provides constant, long-term monitoring over a wide area of the  
31  
32 coast would provide unprecedented insight into the episodic, seasonal and interannual variability of  
33  
34 intertidal areas.  
35  
36  
37  
38

39 An effective and long-established method of monitoring shoreline position and nearshore beach  
40  
41 processes is to use video camera analysis of the nearshore and swash zones (Aarninkhof et al., 2003,  
42  
43 2005; Holland et al., 1997; Holman et al., 1993; Holman and Stanley, 2007; Plant and Holman, 1997;  
44  
45 Santiago et al., 2013; Sobral et al., 2013). Video monitoring has been used successfully to monitor  
46  
47 stretches of intertidal beach at a number of sites around the world, such as during a large European  
48  
49 research project CoastView (Davidson et al., 2007) and improvements continue to be made,  
50  
51 including automated methods that are capable of updating bathymetric maps on a daily basis (Uunk  
52  
53 et al., 2010). The use of thermal infrared cameras allows such methods to be performed using data  
54  
55 collected both during the day and at night to derive intertidal DEM (Digital Elevation Models)  
56  
57  
58  
59 (Gaudin et al., 2009). Video cameras mounted on towers along a shoreline have also been used  
60  
61  
62  
63  
64  
65

1  
2  
3  
4 successfully in combination with in situ sensors to measure morphological change and sediment  
5  
6 transport (Austin and Masselink, 2006) and these passive optical sensors have been proven to be  
7  
8 accurate and effective in their deployment.  
9

### 10 11 **1.3 Depth mapping with marine X-band radar** 12

13  
14 Marine radar generally operates well in low visibility, has excellent temporal and spatial coverage  
15  
16 and is able to provide similar data to that of a camera at slightly lower resolution but to a  
17  
18 significantly greater range and regardless of light conditions (Dankert and Horstmann, 2007). X-band  
19  
20 radar has become an integral part of the nearshore remote sensing infrastructure in recent years  
21  
22 (Holman and Haller, 2013). Operationally, it has been used extensively to determine 2-D wave  
23  
24 spectra in offshore areas for both commercial and scientific applications for many years now (Nieto  
25  
26 Borge and Guedes Soares, 2000; Reichert et al., 1999), for the most part using techniques based on  
27  
28 those developed by Young et al. (1985). The visibility of ocean waves on the radar imagery and the  
29  
30 ability to record sequences of these images of the waves allows their wavelength and period to be  
31  
32 determined. If currents are neglected, various techniques can be used to fit the water depth that  
33  
34 best explains the observed wave behaviour (Bell, 1999, 2008; Bell et al., 2006; Flampouris et al.,  
35  
36 2009; Hessner et al., 1999).  
37  
38

39  
40 If the data are from areas where currents cannot be neglected, it becomes necessary to find the best  
41  
42 fit to the location of the wave dispersion surface in the full 3D wavenumber-frequency domain in  
43  
44 terms of the water depth and the two components of the current vector. Again, there are various  
45  
46 approaches to both determining (and sometimes filtering) the frequency wavenumber spectrum and  
47  
48 also a number of approaches to finding the best fit of the current vector and depth to the observed  
49  
50 wavenumber spectrum (Senet et al., 2008; Hessner et al., 2009, 2014; Nieto Borge et al., 2004, 2008;  
51  
52 Serafino et al., 2010). Such techniques have been used successfully to map currents at tidal energy  
53  
54 test sites in Scotland UK (Bell et al., 2012, McCann & Bell, 2014). Recently, the additional  
55  
56 complication of correcting for vessel movement has started to be addressed in order to allow  
57  
58  
59  
60  
61  
62  
63  
64  
65

1  
2  
3  
4 bathymetry mapping using radar data from a moving vessel, and water depth maps down to a water  
5  
6 depth of approximately 50 m have been shown to be possible (Bell and Osler, 2011).  
7  
8

9 The overriding stipulation for these wave inversion techniques is that clear wave fields must be  
10  
11 visible to the radar in order for the analysis to work accurately. Such techniques also inherently  
12  
13 involve the analysis of data windows of several hundred metres square in order to allow the  
14  
15 determination of the wave properties required to reliably determine both water depth and currents.  
16  
17 Thus a degree of spatial averaging is involved that makes that approach less useful for the mapping  
18  
19 of often high spatially variable intertidal areas.  
20  
21

22 The Temporal Waterline method detailed in the following sections is not as reliant on the presence  
23  
24 of coherent wave patterns on the radar data and operates at a pixel level rather than involving  
25  
26 spatial averaging. The combination of the products of water line and wave inversion methodologies  
27  
28 is planned for future work.  
29  
30

#### 31 32 **1.4 The Temporal Waterline Method** 33

34 The method presented in this paper builds upon known principles, an early version of which was  
35  
36 described by Admiral Sir R.H. Bacon who commanded the UK Dover Patrol from 1915-1917. During  
37  
38 this time he correctly theorised that aerial photographs taken at regular timed intervals over a  
39  
40 shoreline could be used in conjunction with a known tidal levels measured from a submarine to  
41  
42 create a series of contour lines that described elevations above Chart Datum, and thus describe the  
43  
44 beach profile (Bacon, 1932). This knowledge was critical in the planning of amphibious landings and  
45  
46 military operations in the nearshore area. This underlying principle has been applied to a variety of  
47  
48 remote sensing methods, such as Synthetic Aperture Radar (SAR) by Koopmans & Wang (1994) who  
49  
50 picked out the waterlines of the intertidal areas of the Wadden Sea and assigned those contours to  
51  
52 water elevations based on a tidal model. Mason and Davenport (1995) carried out a similar exercise  
53  
54 with SAR images of the extensive intertidal regions of the Morecambe Bay area of the UK. An  
55  
56  
57  
58  
59  
60  
61  
62  
63  
64  
65

1  
2  
3  
4 iterative process was later used between the tidal model and updating bathymetry to arrive at more  
5  
6 precise tidal elevations for the detected waterlines (Annan, 2001).  
7

8 The waterline approach to intertidal mapping has also been applied to marine radar data. Takewaka  
9  
10 (2005) showed that beach elevations could be determined by associating the strong radar echo due  
11  
12 to waves breaking on the shoreline with the tidal elevation recorded nearby. Beach slopes were also  
13  
14 calculated from a number of records separated in time. However, the analysis used by Takewaka  
15  
16 sometimes required manual intervention to correct the waterline estimate and hence was  
17  
18 inappropriate for automated application to large datasets and long time series.  
19  
20

21 Repeated analysis of the same area over varying timescales allows the measurement and  
22  
23 quantification of sediment transport (Mason and Garg, 2001; Mason et al., 1999; Ryu et al., 2008).  
24

25 The source of images is commonly SAR from either satellite or survey aircraft, because the active  
26  
27 sensing ability of SAR allows penetration of cloud cover and the gathering of images during poor  
28  
29 weather, a quality shared by X-band radar. It is also possible to use traditional optical satellite  
30  
31 images to detect waterlines (Ryu et al., 2002), the availability of which can be intermittent, thus  
32  
33 reducing the temporal resolution of the method and leading to increased interpolation errors in the  
34  
35 final map. Recently this method has been used to map large areas of the coast of China with mean  
36  
37 vertical errors in the measurements between 29 – 42cm (Liu et al., 2013). The technique was also  
38  
39 applied using SAR images to map the change in topography on tidal flats along the Wadden Sea  
40  
41 German coast between 1996 and 1999. The elevation values in this region were compared to those  
42  
43 gathered by survey vessel, the mean error was 20cm in 1996 and 21cm in 1999 (Heygster et al.,  
44  
45  
46  
47  
48  
49 2010).

50 The X-band radar waterline method described here differs from those already discussed by moving  
51  
52 the waterline detection from the spatial domain of identifying the discrete waterline in individual  
53  
54 images, to the temporal domain where the transitions between wet and dry are associated with the  
55  
56 best match between pixel intensity records and the tidal signal which would cause that  
57  
58 wetting/drying pattern over a given time period (Bell, 2014). This takes advantage of the excellent  
59  
60  
61  
62  
63  
64  
65

1  
2  
3  
4 temporal update rates possible with ground-based remote sensing but could equally be applied to a  
5  
6 range of remote sensing data types, given a sufficient number of images. More importantly, it  
7  
8 circumvents the need for the waterlines in individual images to be clear and unambiguous – which is  
9  
10 often not the case. Most published methods contain extensive details of error correction methods to  
11  
12 deal with discontinuities in contour lines in individual images or handle ambiguous water lines. With  
13  
14 the temporal approach these are unnecessary, and thus the method is easily automated and  
15  
16 inherently more robust.  
17  
18

## 19 **2. Methodology**

### 20 **2.1. Experiment description**

21  
22  
23  
24 Radar image data were collected using a Kelvin Hughes 9.4GHz horizontally polarised X-band marine  
25  
26 radar mounted on a 15 m mast (Figure 1), itself approximately 15m above chart datum, at Hilbre  
27  
28 Island, northwest UK at the mouth of the River Dee (Figure 2). This site offers good visibility of the  
29  
30 estuary and the north western beach of the Wirral peninsula. The Dee estuary is a funnel-shaped,  
31  
32 macrotidal estuary on the border between North Wales and England with a maximum spring tidal  
33  
34 range of more than 10 m. The site features particularly interesting geomorphology, with a  
35  
36 progressively accreting saltmarsh to the south-east, migrating tidal channels within the central  
37  
38 sandbanks and shifting intertidal bed features along the beach. The waves within Liverpool Bay and  
39  
40 the mouth of the Dee estuary are locally generated and fetch limited within the eastern Irish Sea  
41  
42 such that significant wave height ( $H_s$ ) is less than 5.5 m, the peak wave period ( $T_p$ ) is less than 12 s,  
43  
44 and the mean period less than 8 s (Wolf et al., 2011). The main channel of the River Dee splits into  
45  
46 two deep channels around 12 km downstream from a canalised section leading to the City of  
47  
48 Chester, the Hilbre channel to the east and the Welsh channel to the west, which feed into the  
49  
50 Eastern Irish Sea (Moore et al., 2009).  
51  
52  
53  
54  
55

### 56 **2.2. Radar data collection and pre-processing**

57  
58  
59  
60  
61  
62  
63  
64  
65

1  
2  
3  
4 Hilbre Island, where the radar was located, is cut off from the mainland for the upper half of every  
5  
6 tidal cycle and has no grid-connected electricity supply. In order to provide power to the ranger  
7  
8 station on the island, a 2 kW wind turbine and off-grid battery storage system with diesel generator  
9  
10 back-up was installed by Wirral Borough Council, which provided power most of the time. The  
11  
12 remote nature of the site made maintenance and monitoring of both the power systems and the  
13  
14 radar system a challenge and numerous gaps exist in the dataset as a result. Despite these  
15  
16 challenges, several years of radar data were collected before a number of factors made the data  
17  
18 collection impractical to continue.  
19  
20

21 The radar data used in the present work were gathered over 10 months from March 2006 to January  
22  
23 2007. Further archives of radar data up to 2009 exist and will form the basis of future work  
24  
25 investigating episodic, seasonal and interannual changes within the estuary. The 2.4 m radar  
26  
27 antenna was mounted approximately 30 m above chart datum and set to short pulse (~60 ns pulse  
28  
29 length) in order to cover a 4 km range radius. The data were then sampled at 40 MHz with a radial  
30  
31 resolution of 3.75 m using an OceanWaves GmbH Wamos system linked to the internet via a long  
32  
33 range wi-fi link to the mainland. The antenna rotated at 25 rpm yielding an image every 2.4 s. The  
34  
35 raw data were then interpolated from polar coordinates onto a Cartesian grid to enable  
36  
37 georeferencing and proper visualisation of the results. This process includes the removal of small  
38  
39 variations in antenna rotation rate that would otherwise cause an azimuthal error of several degrees  
40  
41 in the location of nominally static targets if a uniform antenna rotation rate was assumed.  
42  
43  
44  
45

46  
47 Strictly speaking, the polar to Cartesian conversion should also account for the slant range  
48  
49 associated with the elevation of the radar antenna above ground level – a simple calculation using  
50  
51 Pythagoras' theorem. However, as the ground level is the unknown quantity in this analysis, one can  
52  
53 either assume an approximate elevation that accounts for the majority of the slant range error or  
54  
55 include no correction. The option of no correction was chosen in this case as an antenna elevation of  
56  
57 approximately 25-30 m coupled with a Cartesian pixel size of 5m means that the slant range error  
58  
59 only becomes greater than the pixel size for points within approximately 100 m of the radar in a  
60  
61  
62  
63  
64  
65

1  
2  
3  
4 region where data is being recorded to a range of almost 4 km.

5  
6 If precision in the nearest 100 m was of principle concern, the simplest method would be to perform  
7  
8 the waterline method with no slant range correction, and once the elevation of each pixel had been  
9  
10 identified, apply a correction to the radial range of each pixel based on the slant range appropriate  
11  
12 to that elevation and range. A detailed correction for this effect was considered an unnecessary over  
13  
14 complication in the present work considering the likely marginal gains in positional accuracy. It may  
15  
16 however be implemented as a refinement in future work if necessary.  
17  
18

19 Images produced from radar data show not only detected hard targets such as ships and land, but  
20  
21 also many reflections from the sea surface. This is known generally as "sea clutter" and is a product  
22  
23 of Bragg scattering from centimetre-scale capillary waves on the sea surface interacting with the  
24  
25 projected electromagnetic energy (Valenzuela, 1978) and sea spikes, a scattering phenomenon  
26  
27 occurring when radar waves interact with steep or breaking waves at low grazing angles (Coakley et  
28  
29 al., 2001; Fuchs et al., 1999; Ja et al., 2001; Trizna and Hansen, 1991). This sea clutter is  
30  
31 inconsequential for the most part if wind speed is low (<3 m/s). As the sea surface is not roughened  
32  
33 sufficiently, significant wave heights less than 1 m are also difficult to detect with radar. This radar  
34  
35 frequency is also used by weather radars and thus rainfall is also visible on marine X-band radar and  
36  
37 can potentially obscure the sea clutter (Bell et al., 2012). Figure 3 shows a snapshot of radar image  
38  
39 data collected from Hilbre Island. The hard coast of the Wirral mainland is clearly defined to the east  
40  
41 and sea clutter is also detected, particularly along the shoreline to the northeast where breaking  
42  
43 waves give higher radar returns.  
44  
45  
46  
47

48 The intensity of a pixel in a radar image is dependent on the strength of the radar returns from that  
49  
50 location (Richards, 2005) and in marine radars is uncalibrated and usually logarithmically amplified.

51  
52 The raw value of the returned signal is stored as an unsigned 12-bit integer by the particular  
53  
54 digitisation system used here.  
55  
56

57 Sequential radar images recorded once per antenna rotation provide movies of waves (when visible)  
58  
59 propagating up to the shore, and the interface between wet areas and dry areas varies from wave to  
60  
61  
62  
63  
64  
65

1  
2  
3  
4 wave. In order to stabilise this fluctuating signal and define a “waterline” representative enough for  
5  
6 this analysis, the radar images from each ten minute burst (of 256 images) are temporally averaged,  
7  
8 smoothing the wave signatures and yielding an image that is analogous to a time-exposure in  
9  
10 photography, in which the limit of the interface between land and ocean is more easily distinguished  
11  
12 (Figure 4); The time exposure radar images used in this work represent just over 10 minutes of data  
13  
14 that were gathered either every hour or every 30 minutes, depending on the operating regime.  
15  
16 Figure 4 shows a sample time exposure image used in this method. This image represents a period at  
17  
18 low tide and so a great deal of beach is exposed between the shoreline and the seawalls and dunes  
19  
20 along the peninsula to the east of Hilbre Island. The tidal sandbanks to the west are also exposed at  
21  
22 low tide and the repeated wave breaking along the margins of the Hilbre channel picks out the  
23  
24 general shape of the sandbank margins.  
25  
26  
27  
28

### 29 **2.3. Tidal elevation data**

30  
31  
32 The aim of the presented method is to map the intertidal area, which follows a cycle of wetting and  
33  
34 drying governed primarily by the tides and varied local beach morphology. A partial record of tidal  
35  
36 elevation was available from an old tide gauge located on the northernmost tip of Hilbre Island close  
37  
38 to where the radar was located. This tide gauge, which is thought to have existed in various forms  
39  
40 for up to 130 years, was refurbished in its present form by the Mersey Docks and Harbour  
41  
42 Corporation (now Peel Ports) during the 1970s. It consisted of an obsolete float gauge with chart  
43  
44 plotter. The stilling well for the float was cut into the sandstone bedrock of the island and connected  
45  
46 to a subtidal location off the northern end of the island via a lead pipe. A pressure sensor was also  
47  
48 located in the stilling well coupled to a VHF transmitter from which data were automatically relayed  
49  
50 to both the Mersey Docks and Harbour Corporation and to the Proudman Oceanographic Laboratory  
51  
52 (now the National Oceanography Centre). When the Proudman Oceanographic Laboratory moved  
53  
54 from its original site at Bidston Observatory to Liverpool in 2004, the range became too great for line  
55  
56 of sight reception of the VHF signal, so a VHF receiver was connected directly to the radar digitiser  
57  
58  
59  
60  
61  
62  
63  
64  
65

1  
2  
3  
4 PC on Hilbre Island to pick up the tide gauge data from then on whenever the radar was operating.  
5  
6 Unfortunately the inlet pipe had degraded and became increasingly prone to blockages and siltation  
7  
8 in recent years, compromising data quality. It was finally discontinued by Peel Ports in favour of an  
9  
10 offshore radar level gauge in 2010.  
11

12  
13 The available Hilbre Island tide gauge data is shown in Figure 5a with the period that overlaps with  
14  
15 the study period of the present work shown in blue. Figure 5b shows the residual when the tidal  
16  
17 prediction for Hilbre Island is removed from the tide gauge record. There are clear anomalies in  
18  
19 various parts of the record that become obvious in the residuals, notably in spring 2007; towards the  
20  
21 end of 2007; and finally showing almost complete blockage of the system in mid 2008.  
22  
23

24 The incomplete and at times unreliable nature of this record made it unsuitable for use in this  
25  
26 application where a robust and continuous time series of water levels was required. An alternative  
27  
28 approach was therefore adopted taking advantage of the nearest UK National Tide Gauge Network  
29  
30 class 'A' tide gauge outside Gladstone Dock, Liverpool. The residual meteorological contribution to  
31  
32 the tide at Liverpool was determined by subtracting the predicted tide from the measured tide. This  
33  
34 is shown in Figure 5c with the period corresponding to the present study highlighted in blue. The  
35  
36 assumption was made that this meteorological component of the water level was a geographically  
37  
38 wide area effect that could also be used as an approximation for the meteorological component of  
39  
40 the water level at Hilbre Island, 15 km to the west. This was then added to the predicted tide for  
41  
42 Hilbre Island to provide the required water level for the radar waterline analysis, shown in Figure 5d  
43  
44 with the study period again highlighted in blue. In order to verify that this "synthetic tide" was a  
45  
46 better representation of the water elevation than tide predictions alone, tidal records from mid-  
47  
48 September 2006 to mid-February 2007 were subjectively selected as a period when the Hilbre Island  
49  
50 tide gauge was not suffering from significant issues with pipe blockages – i.e. when obvious  
51  
52 anomalies in the tide gauge data and residuals were not evident. It should be noted that the authors  
53  
54 cannot be certain that even this section of the data was not contaminated by pipe blockages, only  
55  
56 that any such effects were small.  
57  
58  
59  
60  
61  
62  
63  
64  
65

1  
2  
3  
4 The tidal residuals for both Liverpool Gladstone Dock and Hilbre Island were calculated by  
5  
6 subtracting the tidal predictions from the measured water levels. As expected, a scatter plot of the  
7  
8 residuals from one gauge compared with the other in Figure 6 shows a strong linear relationship  
9  
10 between the residuals from the two tide gauges, with an  $R^2$  correlation of 0.9, a standard deviation  
11  
12 of less than 0.10 m and a Root Mean Square (RMS) difference of 0.10 m.  
13  
14 Over the same period, the RMS tidal residual of the Gladstone Dock data was 0.37 m, suggesting  
15  
16 that if a similar residual was present on the Hilbre water levels then by applying the tidal residual  
17  
18 from Gladstone Dock to the tidal prediction for Hilbre Island should provide a significantly more  
19  
20 accurate water level than using predictions alone. The residuals from the Hilbre tide gauge data with  
21  
22 respect to the tidal predictions alone were compared with the remaining signal when the synthetic  
23  
24 tide (comprising the Hilbre tidal prediction plus the Gladstone Dock residual) were subtracted,  
25  
26 shown in Figure 5e. With predictions alone, the Hilbre Island RMS residual for the test period of  
27  
28 September 2006 – February 2007 was found to be 0.38 m, while the use of the synthetic tide was  
29  
30 found to reduce this to 0.1 m. This represents a reduction in the difference of almost a factor of 4,  
31  
32 confirming that this approach of adding the residual from the Liverpool tide gauge to that of the  
33  
34 Hilbre Island tidal predictions yields a significantly more accurate representation of the water levels  
35  
36 at that site than predictions alone. A subsection of the tidal data are shown in Figure 7, with the tide  
37  
38 prediction marked as the red dotted line, the Hilbre tide gauge data, which was considered valid  
39  
40 during that period, marked in blue, and the synthetic tide marked as the black dots. The points  
41  
42 marking the synthetic tide can be seen to overlay the tide gauge data (cyan line) almost perfectly.  
43  
44  
45  
46  
47  
48

#### 49 **2.4 LiDAR Ground Truth Survey**

50  
51  
52 An aerial LiDAR survey of the majority of the Dee Estuary was conducted by the UK Environment  
53  
54 Agency on the 8th October 2006, shortly after a significant wave event. The survey was conducted  
55  
56 using an Optech ALTM 3100 LiDAR system flown by a dedicated survey aircraft at an altitude of  
57  
58 approximately 900m. A total of 20 flight lines were flown to cover the estuary between 04:25 and  
59  
60  
61  
62  
63  
64  
65

1  
2  
3  
4 07:26 GMT during which the tidal elevations ranged from 0.72 m to 2.47 m, shown as the region  
5  
6 shaded in grey on Figure 7. Calibration flights were carried out at regular intervals by the system  
7  
8 operators and the last calibration flight prior to this survey was reported to be in June 2006. The  
9  
10 accuracy of this instrument at altitudes of up to 1200 m is quoted by the manufacturer as 0.15 m or  
11  
12 better (1 x standard deviation) with a range resolution of 0.01 m. A ground truth survey conducted  
13  
14 by the Environment Agency as part of this survey showed a root mean square error of 0.071 m  
15  
16 between the LiDAR survey and a GPS ground survey, comprising a systematic error (bias) by the  
17  
18 LiDAR data of -0.052 m and a random error of 0.097 m. These comparisons were within acceptable  
19  
20 tolerance for that instrument.  
21  
22

23  
24 The LiDAR elevation data was supplied as a gridded dataset with a 1m horizontal pixel size.  
25  
26 Reflectivity data were also supplied in a similar format. In order to more closely match the resolution  
27  
28 of the radar data, the 1m gridded elevation data from the LiDAR were mean gridded on a 5 m grid  
29  
30 and elevations were adjusted from Ordinance Datum Newlyn (ODN) to Admiralty Chart Datum (ACD)  
31  
32 corresponding approximately to Lowest Astronomical Tide by adding 4.93 m to the ODN values for  
33  
34 the comparisons presented here.  
35  
36  
37

38  
39 Examination of the original 1m gridded data showed clear evidence of elevations related to the  
40  
41 water surface in wet areas, thus elevation values below 2.5 m relative to chart datum were  
42  
43 eliminated from the comparison as potentially contaminated data points. Examination of the  
44  
45 reflectivity values in these wet areas showed high reflectivity when the laser beam was pointing near  
46  
47 vertical, and very low reflectivity data at lower grazing angles. Features with similar reflectivity  
48  
49 signatures could be identified by eye in the bottom of channels in the sand flats and sand banks,  
50  
51 indicating a strong likelihood that such areas contained pooling water, even near low tide when the  
52  
53 survey was conducted. Filtering out such areas from the LiDAR survey was not attempted as no  
54  
55 unique criteria could be determined for that purpose.  
56  
57  
58

### 59 **3. The Temporal Waterline Method**

60  
61  
62  
63  
64  
65

1  
2  
3  
4 The initial step in this method is to gather time series of individual radar pixel intensities from each  
5  
6 time exposure image across the chosen timescale, in this case two weeks, as shown in Figure 8. For  
7  
8 each x and y coordinate of the time exposure image ( $\bar{I}$ ), the (mean) pixel intensity ( $P$ ) is retrieved  
9  
10 from that location; this is then repeated for each time exposure image, with the values being  
11  
12 separated by  $\Delta t$  - in this case either 30 or 60 minutes.  
13  
14

15 The resulting plot (Figure 9d) shows the raw pixel intensities throughout a two week period, where  
16  
17 periodic episodes of high and low intensities generally indicate tidal cycles of wetting and drying.  
18

19 The value of the radar pixel intensity at the peaks will not be regular as it is a function of local  
20  
21 weather and surface conditions. These include including wind speed (which roughens the sea  
22  
23 surface), wave height and wave direction relative to the radar antenna location, which contribute to  
24  
25 varied backscatter of radar energy from the sea surface.  
26  
27

28 The two week length of the analysis period was chosen to include a full spring-neap cycle, thus  
29  
30 maximising the vertical intertidal range able to be detected by this method, while maintaining a  
31  
32 reasonable temporal resolution through a year. It would be possible to reduce the analysis period to  
33  
34 approximately a week and still maximise the intertidal range experienced at a site, provided the  
35  
36 analysis period was precisely half the exact spring-neap cycle length and synchronised such that  
37  
38 each analysis period covered either the interval from neap to spring or from spring to neap. Periods  
39  
40 less than this could also be used, perhaps even a single tidal cycle, but there would be times when  
41  
42 the analysis period would be focussed only on the smaller intertidal range at neaps, which does not  
43  
44 make best use of this overall approach.  
45  
46  
47

48 In order to relate the tidal variation in pixel intensity at a given location to an elevation, a set of  
49  
50 water levels was chosen reflecting the potential tidal range of the deployment area; for Hilbre Island  
51  
52 this was 0.5-10 m in 10 cm increments. For each of these elevations, the synthetic tidal record was  
53  
54 used to determine whether a pixel at that elevation would be either covered by the tide, or exposed  
55  
56 at the times corresponding to each radar record. This yielded a binary pulse sequence unique to  
57  
58 each elevation, illustrated in Figure 9b. Peaks in the absolute gradient of that binary pulse sequence  
59  
60  
61  
62  
63  
64  
65

1  
2  
3  
4 (Figure 9e) represent the points of transition between wet and dry at a given elevation.

5  
6 The example pixel intensity time series shown in Figure 9d is not a clean binary pulse sequence like  
7  
8 the one generated by the tidal record in Figure 9c, due to changing weather and surface conditions  
9  
10 over the two week analysis period. Further, the presence of strong radar reflectors such as rocks in  
11  
12 some pixels can exhibit a high radar cross section that is then reduced by inundation with water,  
13  
14 thus inverting the expected pulse sequence.  
15  
16

17  
18 In order to allow a more like for like comparison between the binary sequences of Figure 9c and the  
19  
20 analogue time series in Figure 9d, we attempt to normalise the analogue time series. The absolute  
21  
22 gradient of the time series is calculated and the gradient peaks selected (representing sharp changes  
23  
24 in intensity) using a robust peak-finding algorithm described by Yoder (2009); these peak values  
25  
26 were then normalised and other non-peak values reduced to zero (Figure 9f). Similarly, the absolute  
27  
28 gradient is also taken of the binary wet-dry pulse sequences, illustrated in Figure 9e.  
29  
30

31  
32 It is then a straightforward matter to step through each possible elevation and determine a measure  
33  
34 of similarity between the theoretical and measured pulse sequences. In this case we use the  
35  
36 normalised cross correlation to calculate  $R$ , the correlation coefficient at each elevation being:  
37  
38

$$R_N = \left\{ \frac{(P - \bar{P})(T_N - \bar{T}_N)}{\sigma_P \sigma_{T_N}} \right\} \quad (1)$$

39  
40  
41  
42 The normalised correlation coefficient ( $R$ ) for each water-level number ( $N$ ) is calculated using  
43  
44 equation (1), where  $P$  is the pixel intensity gradient record and  $T$  is the record of tidal state change  
45  
46 gradients,  $\sigma_P$  and  $\sigma_T$  indicate the standard deviation of  $P$  and  $T$ , respectively.  
47

48  
49 Each tidal elevation value now has a correlation coefficient ( $R$ ) value defining the strength of the  
50  
51 relationship between the record of pixel intensity gradients and the expected wetting and drying  
52  
53 pattern at a given individual pixel location (Figure 10). The maximum coefficient is used to indicate  
54  
55 the tidal elevation of the waterline and the process is repeated for all pixel intensity records from  
56  
57 every pixel location in the input image sequence. The results are then used to populate a matrix  
58  
59 which builds up a map of intertidal pixel elevations above chart datum.  
60  
61  
62  
63  
64  
65

1  
2  
3  
4 It can be seen from Figure 9d and the derived pulse sequence in Figure 9f that there are times when  
5  
6 the transition between wet and dry is not evident in the data, probably due to very calm weather  
7  
8 conditions. If one attempted to apply the conventional approach of identifying a physical waterline  
9  
10 in the radar images from records around that time, it would not be possible because that  
11  
12 information is not contained within the data. However, by taking the temporal approach to the  
13  
14 problem, provided there are at least some measurable wet-dry transitions during the two week time  
15  
16 period, the absence of even days of wetting and drying transitions can be tolerated as can the  
17  
18 occasional erroneous identification of a transition caused by for heavy rain for example.  
19  
20

21 Pixel records from areas which are submerged even at low tide (subtidal areas) generally yield low  
22  
23 correlation coefficients with the predicted wetting & drying pulse sequences. These areas are  
24  
25 filtered out by setting a simple threshold in the correlation coefficient as a quality control. The  
26  
27 resulting maps can be used to visualise the mean elevations over a single spring neap cycle.  
28  
29  
30

#### 31 **4. Results**

32  
33  
34 The Temporal Waterline method described above was used to process radar data from March 2006  
35  
36 – January 2007. For each two week period during that time, the analysis yielded both an elevation  
37  
38 map corresponding to the wetting and drying transitions and also a corresponding correlation  
39  
40 coefficient map reflecting the confidence level of the estimated elevations at each pixel location.  
41  
42

43 An example of a correlation map from April 2006 is shown in Figure 11. Pixels with higher correlation  
44  
45 values should provide a more reliable elevation estimate, whilst lower correlation points should  
46  
47 potentially be removed as a quality control measure. Generally, the non-mobile areas generate very  
48  
49 strong correlations, for example the rock armouring and sea wall of a recreational marine lake to the  
50  
51 south-east is picked out clearly on the image with high correlation values of approximately 0.8, along  
52  
53 with the well-established sandbanks and isolated rocks across the estuary. Lower correlation values  
54  
55 of 0.3 or less are seen in the areas which are still submerged at low tide as these areas should not  
56  
57 exhibit a tidal fluctuation that corresponds with wetting-and-drying.  
58  
59  
60  
61  
62  
63  
64  
65

1  
2  
3  
4 Radar data collection is inhibited through shadowing , a phenomenon common in the analysis of  
5  
6 ocean waves with low-grazing angle radar (Lynch and Wagner, 1970; Mattie and Harris, 1978). Even  
7  
8 with the radar being sited on a tower, the large radial range over which data has been recorded  
9  
10 means that some intertidal areas will still be shadowed from the radar signal, and these areas also  
11  
12 exhibit low correlations. Clear, unobstructed line of sight to the intertidal area of interest is  
13  
14 therefore an important consideration when selecting a deployment site. A subjectively chosen  
15  
16 correlation threshold of 0.3 was used to filter out the values generally corresponding to subtidal and  
17  
18 shadowed areas as a quality control process. Land areas and the islands have been masked out and  
19  
20 set to an arbitrary elevation above the maximum tide.  
21  
22

23  
24 A single waterline map is shown in Figure 12 illustrating the mean intertidal bathymetry over a two-  
25  
26 week period; successive analyses over a longer time period will be useful in isolating and monitoring  
27  
28 the movement of bed features over different timescales. The intertidal sand flats of West and East  
29  
30 Hoyle Bank are clear in Figure 12, as are the banks of the large central channel. This is one of two  
31  
32 channels into the Dee estuary which connect to the canalised River Dee and the city of Chester 20km  
33  
34 higher up the estuary. A striking result is that the wreck of the Greek cargo ship SS Nestos displayed  
35  
36 in Figure 13, stranded and sunk on the sandbank in 1941, can be seen clearly to the north, with an  
37  
38 elevation of ~3.5 m at low tide.  
39  
40  
41

#### 42 **4.1. Temporal filtering and smoothing of elevation values**

43  
44

45  
46 The elimination of pixels by any quality control process would lead to unwanted gaps in individual  
47  
48 elevation maps. It would not be appropriate to spatially interpolate the missing values as the  
49  
50 gradient of complex beach profiles is rarely linear and assuming such could lead to significant errors  
51  
52 in further processing (Holman and Bowen, 1979).  
53

54  
55 However, the existence of multiple sequential records allows an alternative approach to be taken to  
56  
57 mitigate and filter points with intermittent poor correlations. A weighted temporal smoothing of the  
58  
59 time series of each pixel was applied to the ten months of results. The square of the correlation  
60  
61  
62  
63  
64  
65

1  
2  
3  
4 coefficients was used to weight each elevation at each two-week time step in a five point running  
5  
6 smoothed fit using a robust smoothing algorithm by Garcia (2010). This has the effect of strongly  
7  
8 smoothing the resulting time series of elevations while emphasising points with good correlations  
9  
10 and de-emphasising those with weak correlations. An example of the results of smoothing the data  
11  
12 in this way can be seen later in Figure 16b  
13  
14

#### 15 4.2 Physical meaning of the waterline

16  
17  
18  
19 The algorithm described here operates in the time domain rather than the spatial domain, hence it is  
20  
21 not immediately obvious how the derived waterline relates to an individual record. Figure 14 gives  
22  
23 an example of how the derived waterline relates to both the LiDAR survey and the wave signatures  
24  
25 on an individual radar record along a cross shore transect. The record started at 06:00 on the 6<sup>th</sup>  
26  
27 October 2006 and finished at around 06:10 after recording 256 images under relatively low wave  
28  
29 conditions, just before a significant wave event. A cross-shore transect from the radar backscatter  
30  
31 time series, and corresponding to transect 2 in Figure 15, is shown in the plot as it progresses  
32  
33 through just over 10 minutes of data. The left hand side of the plot corresponds to the onshore (dry)  
34  
35 sand flats while the right hand side has the sea clutter of the waves approaching from right to left.  
36  
37 The tidal elevations at the start, middle and end of the record were 2.97 m, 3.11m and 3.29m  
38  
39 respectively. Figure 14a shows how the radar backscatter profile evolves over the ten minutes, with  
40  
41 the wave breaker line clearly evident around  $x = 550$  m, and the change in water level on the  
42  
43 location of the breaking waves on the beach profile is immediately evident, with the breaker line  
44  
45 having moved approximately 25m as the water level rose by over 30cm during that time. Shoreward  
46  
47 of the breaker line to the left, there are some strong backscatter targets that appear to move  
48  
49 around, and inspection of the full radar image sequence verified that these are almost certainly sea  
50  
51 birds moving around either singly or in groups on the sands. Figure 14b shows the temporal mean of  
52  
53 that backscatter profile. The cyan line marked on both plots indicates the location where the still  
54  
55 water level with respect to the LiDAR survey in the middle (at 06:05 am) of the radar record would  
56  
57  
58  
59  
60  
61  
62  
63  
64  
65

1  
2  
3  
4 lie. The red, green and blue lines mark the corresponding derived average waterlines from the 2  
5  
6 week period ending on the 8<sup>th</sup> October 2006, and at the start, middle and end of the 06:00 - 06:10  
7  
8 6<sup>th</sup> October 2006 record respectively. The line corresponding to the middle of the radar record in  
9  
10 time (green line) is close to the peak of the backscatter associated with the breaker line, which  
11  
12 corresponds well with the peak of the breaker backscatter used as the criterion for defining the  
13  
14 water line used by Takewaka (2005).  
15  
16

17  
18 Since the waterline derived here relates to the peak in the shore breaker zone, it is slightly offshore  
19  
20 of that which might be expected from the LiDAR elevation plus still water level at that time, which is  
21  
22 the factor generating the slight overestimate in overall beach elevations described later.  
23  
24

#### 25 26 **4.2. Changes in beach transects**

27  
28 Figure 15 shows the location of five cross-shore transects extracted from the processed dataset.

29  
30 These transects capture most of the foreshore beach extending from the subtidal boundary to the  
31  
32 backshore where the gradient decreases. Transect 5 is the northernmost, with transect 1 being  
33  
34 closest to the Island.  
35

36  
37 Figure 16 shows the results of extracting these transects every two weeks from 10 months of data,  
38  
39 each row represents elevations along the transect from on to offshore. Noisy data appears most  
40  
41 prominently across all transects around time step 10 and 17 (29/07/2006 and 4/11/2006). This could  
42  
43 be the result of very calm weather during the two-week sample periods, resulting in a smoother sea  
44  
45 surface (i.e. less sea clutter) and lower correlation coefficients. The mean offshore significant wave  
46  
47 heights for these time steps were 0.66 m and 0.82 m according to the CEFAS Wavenet buoy (WMO  
48  
49 ID:62287) in Liverpool Bay compared to a mean of 0.92 m and a maximum of 4.89 m seen in January  
50  
51 2007 (these wave data are accessible from <http://www.cefas.defra.gov.uk>). Waves of this height (<1  
52  
53 m) are difficult to detect with marine radar (although the wave heights will have increased as the  
54  
55 waves shoal), so it is unsurprising that the data are poor for these periods. From Figure 15 it is clear  
56  
57 that transect 5 runs close to a channel in the sand flats where shadowing inhibits the radar line of  
58  
59  
60  
61  
62  
63  
64  
65

sight. Figure 17 shows the start and end transects from the ten months of data, which demonstrate that there is evidence of changes to the beach level during that time and that those changes in beach profile are quantifiable from the waterline derived topographic maps. Although there are small sections of the beach that move seawards and that appear to be associated with the crests of large bedforms, the overall pattern of change is a mean shorewards migration of the beach profile, which may be a seasonal effect rather than a long term trend of erosion.

Table 1 lists the mean changes both in elevation along the transects and horizontally in terms of the cross shore translation of the beach profile from the beginning to the end of the ten-month period.

Vertical elevation changes averaged over each profile range from an erosion of 0.05 m at the transect furthest from the radar to an erosion of 0.17 m at the transect nearest the radar. These are relatively small overall changes in bed level, but due to the shallow profile of the beach, these translate to considerable shorewards translation of the beach profile by between 25 m (furthest) and 40 m (nearest). The vertical variations are well within subjective observations by one of the authors of considerable variations in beach level relative to the rocks adjacent to Hilbre Island of significant fractions of a metre. Future work will use a larger 3 year dataset to investigate seasonal and inter-annual variations in the beach elevations and track large sediment waves/dunes as they evolve and migrate.

<b>Transect</b>	<b>Mean Vertical change (m) from March 2006 to January 2007</b>	<b>Mean Horizontal change (m)</b>
<b>1 (nearest to radar)</b>	-0.17	-37.7
<b>2</b>	-0.10	-30.3
<b>3</b>	-0.16	-39.6
<b>4</b>	-0.10	-30.8
<b>5 (furthest from radar)</b>	-0.05	-24.9

1  
2  
3  
4 **Table 1. Mean beach profile changes for profiles 1-5 in terms of elevation and cross shore**  
5  
6 **horizontal translation. All transects show a small (<0.2 m) mean reduction in elevation over the ten**  
7  
8 **months, with corresponding mean values for the cross shore translation of the beach profile that**  
9  
10 **are large due to the shallow (approximately 1 in 250) nature of the beach gradient.**

11  
12  
13  
14 It is further noted that the changes in the transects over time strongly suggest the presence of  
15  
16 migrating intertidal sand bars or waves, the dimensions and movements of which could be  
17  
18 quantified with this technique. Studies by McCann (2007) and Way (2013) have previously  
19  
20 documented the length and migration rates of these sedimentary bedforms but the profiles could  
21  
22 not be remotely determined with the earlier approach. These features have wavelengths of the  
23  
24 order of 100 m - 200m and have been observed to migrate in excess of 100 m per year landwards  
25  
26 using the radar signatures of breaking waves over the waves as a proxy indicator for their position. It  
27  
28 is hoped that the ability to measure sediment volume changes cost effectively over long time  
29  
30 periods will allow variations in sediment fluxes within the surveyed area to be quantified effectively.  
31  
32  
33 This idea will be explored in further work.

#### 34 35 **4.3. Fixed elevation control points**

36  
37  
38 The changes observed in these transects demonstrate that the method is capable of determining  
39  
40 surprisingly small changes in beach elevations provided the changes are real and not artefacts of  
41  
42 seasonal changes in wave height. To investigate this possibility, a number of rocky outcrops in the  
43  
44 intertidal zone were chosen as control points that should not vary in elevation. If the results showed  
45  
46 that that these targets did not vary in elevation through the ten months of the study period, then it  
47  
48 would be reasonable to assume that changes in the elevations of potentially mobile sandy areas  
49  
50 nearby during the same period are genuine.  
51

52  
53  
54 The locations of these control points are shown in Figure 18. One site is located on Hilbre Island  
55  
56 itself, another on a rock Platform close to the Island, one from Hilbre Middle Eye, and the final site is  
57  
58 from the rock armour protecting the recreational marine lake at West Kirby.  
59  
60  
61  
62  
63  
64  
65

1  
2  
3  
4 The time series of waterline-derived elevations for each control point are displayed, with waterline  
5  
6 elevation relative to Admiralty Chart Datum (m) on the y axis and time in two week intervals along  
7  
8 the x axis. The plots show that radar derived elevations at these control points are relatively stable  
9  
10 across 10 months, and thus it is concluded that the elevation changes observed in the sandy areas  
11  
12 are almost certainly genuine.  
13

#### 14 **4.4. Relationship between the waterline elevation and the absolute intertidal elevation**

15  
16 It should be emphasised that the elevations determined by this method are those of the waterline  
17  
18 relative to the tidal water level. This is not the same as the absolute elevation that might be  
19  
20 surveyed by LiDAR or other survey methods. However, the purpose of beach transects and surveys  
21  
22 themselves should be considered before a discussion of relative accuracies of one method against  
23  
24 another. The purpose of many beach transect monitoring campaigns is to determine to what  
25  
26 position the combination of waves and tides might reach, damage sea defences and potentially  
27  
28 overtop beaches and sea walls. Conventional surveys are carried out to absolute elevation datums,  
29  
30 then tidal elevations can be combined with models of wave setup and runup to estimate how high  
31  
32 up the beach the water would reach under various conditions. Waterline methods potentially supply  
33  
34 this information directly, without the need for the modelling step, so absolute accuracy of the  
35  
36 waterline derived elevations relative to a survey may be less important than the long term stability  
37  
38 of the technique.  
39  
40  
41  
42

43  
44 Figure 19a shows the elevations determined by the Temporal Waterline method cropped to the  
45  
46 areas covered by the October 2006 LiDAR survey. Figure 19b shows the LiDAR survey itself. The  
47  
48 general shape, location and elevations of the coastline and sandbanks detected by the waterline  
49  
50 method are in mostly in good agreement with the LiDAR survey. There is an area of particularly poor  
51  
52 results to the southwest of the study area in Figure 19a where the radar method overestimates bed  
53  
54 elevation by in excess of 5 m in places. These areas were therefore removed in order to prevent  
55  
56 contamination of further analysis. A combination of the shadowing effect of the sandbanks at mid-  
57  
58 to low tide and the increasing lack of sea clutter at locations further into the sheltered estuary is  
59  
60  
61  
62  
63  
64  
65

1  
2  
3  
4 thought to be the cause of the concentrated area of poor results. It is, however, significant that the  
5  
6 present processing and filtering techniques do not remove these poor elevations and the pixel  
7  
8 records in these areas often have seemingly valid matches with a given tidal elevation. Identifying  
9  
10 the reason for this and addressing the issue is a priority for future work.

11  
12 In order to quantify the differences between the LiDAR and radar elevation plots, the LiDAR values at  
13  
14 each point were subtracted from the radar derived values. Figure 20 shows these residuals. The  
15  
16 majority of the radar-derived elevations lie within  $\pm 1$  m of the corresponding LiDAR elevations, with  
17  
18 the overall pattern indicating that the waterline derived elevations are slightly higher than the  
19  
20 survey elevations. Intuitively this might be expected due to contributions from wave setup and  
21  
22 survey elevations. Intuitively this might be expected due to contributions from wave setup and  
23  
24 runup. However, the steeper beachfaces within 2 km of the island show surprisingly good agreement  
25  
26 with the LiDAR survey, which may indicate that the wave runup and setup may not be the only  
27  
28 factors involved in the differences.

29  
30 Consistent differences between survey and waterline elevations with strong correlation values are  
31  
32 evident over the flatter areas of the sand banks. This suggests there may be additional effects that  
33  
34 add to the elevation of the water, such as pooling of the water between sediment features.

35  
36 Figure 21 shows a comparison between the waterline derived elevations and the corresponding  
37  
38 LiDAR transects. These reveal that the sloping parts of the transects leading down to the low water  
39  
40 mark are relatively well matched between LiDAR and waterline. However, the flatter areas bounded  
41  
42 by sediment bars or sand waves appear have water trapped behind the bedforms, supporting the  
43  
44 idea that water is pooling on the sand flats and creating some of the differences between LiDAR and  
45  
46 waterline maps. As has already been noted, the reflectivity data associated with the LiDAR  
47  
48 elevations also indicated pooling of water in these areas, even at low water.

49  
50 This is an effect known to exist by the authors, based on numerous trips walking to the island. As the  
51  
52 tide goes out, it takes a considerable time for the water to drain off the flatter areas, and it is often  
53  
54 advisable to wait an hour or two beyond the time when the tide has nominally gone out to allow  
55  
56 sufficient water to drain off the sand flats before setting off for the island on foot.  
57  
58  
59  
60  
61  
62  
63  
64  
65

1  
2  
3  
4 These factors indicate that the simplification of applying the water level associated with the tide  
5  
6 gauge location on Hilbre Island across the whole domain is probably an over-simplification.  
7

#### 8 **4.5. Close-range (< 3 km range) accuracy**

9

10  
11 In order to better compare the features present in the LiDAR and radar-derived elevations and the  
12  
13 spatial distribution of differences at the closer range, Figure 22 shows a subsection of the data  
14  
15 covering the area of the northeastern beach in more detail. Figure 22 (a) shows the radar derived  
16  
17 waterline results; (b) shows the LiDAR survey; (c) the difference between the waterline and LiDAR  
18  
19 elevations and (d) the areas likely to be shadowed based on ray tracing and the LiDAR survey. It is  
20  
21 clear from the difference plot in Figure 22(c) that the waterline method determines absolute  
22  
23 elevations along the immediate eastern and southern beach very well. Areas further from the radar  
24  
25 and thus also further from the location relating to the water level data show an increasing over  
26  
27 estimate in the elevations compared with the LiDAR survey. Some areas of the sand flats are  
28  
29 shadowed from the radar, as illustrated by the shadow plot in Figure 22d, calculated from the LiDAR  
30  
31 survey using a simple ray tracing approach. Thus elevations calculated for these areas are not likely  
32  
33 to be accurate.  
34  
35  
36  
37

38 Figure 23 shows a series of error histograms comparing the LiDAR elevations with those of the  
39  
40 Temporal Waterline at different ranges from the radar. The region within 0.75 km of the radar  
41  
42 location (Figure 23a) exhibits a mean bias of 0.12 m higher than the LiDAR survey, while the regions  
43  
44 from 0.75 km range to 1.5 km range (Figure 23b); from 1.5 km - 2.25 km (Figure 23c) and from 2.25  
45  
46 km – 3 km (Figure 23d) exhibit a greater bias of 0.52 m. The 0.48 m and 0.59 m respectively. These  
47  
48 regions encompass more of the flatter areas of sand flats. This reinforces the conclusions from  
49  
50 Figure 21 suggesting these flatter areas consistently experience pooling water, and also include  
51  
52 larger areas shadowed from the view of the radar which are likely to have erroneous values.  
53  
54  
55

56  
57 Further errors might be expected due to the simplification that the tidal elevation relating to the  
58  
59 location of the Hilbre Island tide gauge defines the water level across the entire analysis area. The  
60  
61  
62  
63  
64  
65

1  
2  
3  
4 true pattern of water elevation across this complex macro-tidal environment must be expected to  
5  
6 degrade with range from the measurement location. Moore et al. (2009), explored the differences in  
7  
8 tidal asymmetry across the estuary via a numerical modelling study, showing stronger asymmetry  
9  
10 over the sand banks compared with the channels, which confirms that our assumption of a uniform  
11  
12 tidal elevation across the site at any particular moment is almost certainly an over-simplification.  
13  
14 Attempts to apply a more realistic 2-D tidal elevation pattern either using a tidal propagation model  
15  
16 or empirically may be explored in future work. In particular, the issue of pooling water taking time  
17  
18 to drain off the sand flats might suggest that although the transition time of the rising tide may be  
19  
20 relatively accurate across the study site, that of the falling tide may be delayed relative to the tide  
21  
22 gauge location.  
23  
24

25  
26 Some differences between the radar derived elevations and the survey are also to be expected due  
27  
28 to the different temporal scales of the two surveys. LiDAR is a near instantaneous snapshot in time  
29  
30 whereas radar-derived elevations represent the mean conditions over a two week period in this  
31  
32 case. Thus numerical comparisons must be considered in this light and a perfect match should not  
33  
34 be expected. Significant changes to the shape and location of the sedimentary features have been  
35  
36 observed to occur overnight by the authors, so the superficial features of the intertidal sand flats  
37  
38 must be assumed to be varying slightly even from tide to tide under dynamic conditions. Such  
39  
40 observations reinforce the value of what could be considered a more representative average  
41  
42 measure of intertidal elevations than the snapshots provided by surveys such as LiDAR.  
43  
44  
45  
46

#### 47 **4.6. Cumulative changes in elevation**

48  
49 Figure 24 shows the cumulative variations in radar-derived waterline elevations at each point in the  
50  
51 sand flats region of the domain over the course of the 10 months, the green areas showing a high  
52  
53 degree of stability. The most stable areas located around the landmass of Hilbre Island and the  
54  
55 Peninsula represent concentrations of rocks. In addition, large swathes of the beach are clearly  
56  
57 stable, suggesting a lack of medium-term sediment mobility over those regions. Regions with higher  
58  
59 values of maximum difference in elevation through time are indicative of erosion or deposition. For  
60  
61  
62  
63  
64  
65

1  
2  
3  
4 example, the linear features seen across the beach face potentially mark out the migration of sand  
5  
6 bar features, while areas of high change that are less linear may highlight areas subject to spatially  
7  
8 discrete erosion or accretion. Overall, the plot illustrates that the majority of the area exhibits  
9  
10 relatively little change over the ten months, with isolated areas of mobile features representing  
11  
12 largely superficial changes to that part of the estuary.  
13  
14

## 15 **5. Discussion**

16  
17  
18 This new method of deriving maps of the intertidal zone, although relatively effective and simple in  
19  
20 concept, relies on a number of assumptions that are probably over-simplifications at present.  
21  
22

23 The use of a single instantaneous tidal elevation across a complex estuarine environment is  
24  
25 acknowledged by the authors to be a simplification of reality, and appropriate tidal propagation  
26  
27 models may in future provide a more realistic spatially varying water level distribution across large  
28  
29 areas. In particular, increasing tidal asymmetry across the sand flats and sand banks may be  
30  
31 adversely affecting results in this complex area as a result of this assumption.  
32  
33  
34

35 The present study was conducted in a macro-tidal estuary, in which there are extensive intertidal  
36  
37 areas. At sites where a more modest intertidal zone is expected, consideration must be given to the  
38  
39 expected width of the intertidal zone relative to the radar pixel size. If the intertidal beach width is  
40  
41 narrow relative to the radar pixel size of 5-10 m, then X-band radar may not possess the appropriate  
42  
43 horizontal resolution for the task. Instead, millimetre wave radar such as the 77 GHz version used by  
44  
45 Bell et al (2006) may be more appropriate as such systems are capable of sub-metre range  
46  
47 resolution and have been demonstrated to respond well to the breaking waves and beach run-up  
48  
49 that categorises the water line. Optical camera systems are also likely to work well with this  
50  
51 technique and can provide similar sub-metre resolution within a reasonable range of the camera,  
52  
53 albeit in daylight and good visibility.  
54  
55  
56  
57  
58  
59  
60  
61  
62  
63  
64  
65

1  
2  
3  
4 Further, if the vertical tidal range is narrow, the elevation intervals used in the analysis could be  
5  
6 made finer than the 0.1 m intervals used here. Even in micro-tidal areas, meteorological effects can  
7  
8 introduce significant water level changes in excess of the astronomical tides, and the additional  
9  
10 contribution of these would undoubtedly assist the success of the technique at such sites.  
11

12  
13 The accuracy of the method at the limits of the tidal range also requires further consideration. This is  
14  
15 because the number of waterline transitions close to the water level limits of the spring-neap cycle  
16  
17 will reduce, from the peak of a uniform two transitions per tidal cycle, i.e. over 50 transitions in 14  
18  
19 days, down to single figures and then none as the water level approaches and goes beyond the  
20  
21 limits. Looking for a correlation between the radar derived signatures and a tidally derived signal  
22  
23 with only a few transitions will inevitably result in a less reliable match, and it would be prudent to  
24  
25 implement a threshold in the number of wet-dry transitions below which any derived elevations are  
26  
27 considered at least suspect if not invalid, regardless of the quality of the numerical match achieved.  
28  
29 It may be that the mean low water and mean high water levels would provide standardised  
30  
31 thresholds for this application in the future.  
32  
33

34  
35 The temporal update rate was set to two-week intervals corresponding to a single spring-neap cycle  
36  
37 and chosen to maximise the tidal range during each temporal analysis window. Further work may  
38  
39 investigate reducing this interval to approximately a week or even less but should be synchronised  
40  
41 to span neaps to springs or springs to neaps to ensure the maximum tidal ranges were experienced  
42  
43 during each analysis period.  
44  
45  
46

## 47 48 **Conclusions** 49

50  
51 A new method of analysing the location of waterlines in remotely sensed data has been presented.  
52  
53 The method differs from established methods by moving the problem from the spatial domain to the  
54  
55 time domain and looking for matches in the expected temporal pattern of transitions between wet  
56  
57 and dry areas over a spring-neap cycle. This is inherently more robust and easier to implement  
58  
59  
60  
61  
62  
63  
64  
65

1  
2  
3  
4 automatically than attempting to identify the precise physical waterline in individual remotely  
5  
6 sensed images. The accuracy relative to a LiDAR survey varies from an overestimate of 0.12 m  
7  
8 within the first 0.75 km from the radar, to an approximate 0.5 m overestimate further from the  
9  
10 radar, although these comparisons are complicated by the complex nature of the macrotidal estuary  
11  
12 used as the test case.  
13

14  
15  
16 The tidal water level used for the analysis is assumed to be flat across the study area at any instant  
17  
18 in time, which is almost certainly an over-simplification, and the application of a modelled 2-D water  
19  
20 level that took into account the tidal asymmetry over sand flats and sand banks may improve the  
21  
22 absolute accuracy in future.  
23

24  
25  
26 The method provides a map of the elevation of the waterlines relative to the tidal reference, rather  
27  
28 than the absolute elevation of the bed. The analysis of pixels corresponding to a number of rocks  
29  
30 demonstrated that elevations of the derived waterlines relating to those rocks are relatively stable  
31  
32 through the 10 months of processed data. In contrast, inspection of a number of beach transects  
33  
34 showed gradual evolution of those transects during the study period, with all beach transects  
35  
36 exhibiting a slight lowering of the beach face during the 10 months from March 2006 to January  
37  
38 2007. Hence, the waterline elevations can be viewed as a very effective measure of intertidal change  
39  
40 yielding volumetric changes that could be used in conjunction with a single validation survey to  
41  
42 relate such changes to absolute elevations if necessary.  
43  
44

45  
46  
47 Despite these simplifications, the results are remarkably stable through time, suggesting that the  
48  
49 method would be suitable for the autonomous monitoring of changes to large intertidal areas over  
50  
51 sustained periods of months to years.  
52

53  
54  
55 In commercial operation, the results from this method could be coupled with bathymetric survey  
56  
57 data of navigation channels to create an integrated chart system, which would populate sub-tidal  
58  
59 areas using data from conventional survey methods, and intertidal zones with waterline derived  
60  
61  
62  
63  
64  
65

1  
2  
3  
4 information. This would potentially provide regularly updated reports on sediment flux and channel  
5  
6 migration. That said, the waterline method is effective as a stand-alone tool for monitoring changes  
7  
8 in the inter-tidal channel margins. This combined mapping strategy may be a vital source of data for  
9  
10 coastal stakeholders and port authorities operating in areas where sedimentary features are mobile  
11  
12 across the intertidal area and those where sediment accretion or erosion in between cycles of  
13  
14 commissioned surveys and maintenance is causing problems in the management of the coast.  
15  
16

### 17 **Acknowledgements**

18  
19  
20  
21 The authors would like to thank Wirral Borough Council's Ranger Service and in particular the (then)  
22  
23 Hilbre Island Ranger - Mr David Cavanagh, for many years of enthusiastic help with numerous  
24  
25 aspects of installing and maintaining a remote system in such a challenging location. Thanks are due  
26  
27 to Mr John M. X. Hughes for the photograph of the SS. Nestos exposed at low tide used in Figure 13  
28  
29 and a set of insightful pilotage notes for the Dee Estuary. The radar data were collected by the  
30  
31 *National Oceanography Centre (NOC) Liverpool* under the umbrella of the *Liverpool Bay Coastal*  
32  
33 *Observatory* and was funded by the *UK Natural Environment Research Council*. Cai Bird's PhD study  
34  
35 was funded by the *Centre for Global Eco-Innovation (CGE)* through the *European Regional*  
36  
37 *Development Fund (ERDF)* and *Marlan Maritime Technologies*. The authors would also like to thank  
38  
39 the anonymous reviewers, whose comments were extremely helpful in improving the content of this  
40  
41 paper.  
42  
43  
44  
45

### 46 **Literature cited**

47  
48 Austin, M. J., & Masselink, G. (2006). Observations of morphological change and sediment transport  
49  
50 on a steep gravel beach. *Marine Geology*, 229(1), 59-77. DOI: 10.1016/j.margeo.2006.02.003  
51  
52 Aarninkhof, S.G., Turner, I.L., Dronkers, T.D., Caljouw, M., Nipius, L., 2003. A video-based technique  
53  
54 for mapping intertidal beach bathymetry. *Coast. Eng.* 49(4), 275–289. DOI: 10.1016/S0378-  
55  
56 3839(03)00064-4  
57  
58 Aarninkhof, S.G.J., Ruessink, B.G., Roelvink, J.A., 2005. Nearshore subtidal bathymetry from time-  
59  
60 exposure video images. *J. Geophys. Res.* 110 (C06011). DOI: 10.1029/2004JC002791  
61  
62  
63  
64  
65

1  
2  
3  
4 Annan, J., 2001. Hindcasting Coastal Sea Levels in Morecambe Bay. *Estuar. Coast. Shelf Sci.* 53, 459–  
5 466. DOI: 10.1006/ecss.1999.0626  
6

7 Bacon, Sir R., 1932. *The Concise Story of the Dover Patrol*. Hutchinson & CO. LTD., London, UK.  
8

9  
10 Bailey, M., 2009. Report on the state of the navigation of the River Mersey. Department for  
11 Transport. Mersey conservancy. Port of Liverpool. Available at:  
12 <http://assets.dft.gov.uk/publications/report-on-navigation-of-river-mersey-2009/report.pdf>  
13 Date accessed: 08/08/14  
14

15 Bell, P.S., 2008. Mapping shallow water coastal areas using a standard marine X-band radar. In:  
16 *Hydro8*, Liverpool, 4th-6th November. 2008. Liverpool, International Federation of Hydrographic  
17 Societies.  
18

19  
20 Bell, P.S., Lawrence, J., Norris, J., 2012. Determining currents from marine radar data in an extreme  
21 current environment at a tidal energy test site. In: *Geoscience and Remote Sensing Symposium*  
22 (IGARSS), 2012 IEEE International Conference. Munich. 22–25.  
23

24 Bell, P.S., Williams, J., Clark, S., 2006. Nested radar systems for remote coastal observations. *J. Coast.*  
25 *Res. Special Issue Proceedings 8th International Coastal Symposium (ICS 2004)* 1, 483–487.  
26  
27

28 Bell, P.S., 1999. Shallow water bathymetry derived from an analysis of X-band marine radar images  
29 of waves. *Coast. Eng.* 37, 513–527.  
30 DOI: 10.1016/S0378-3839(99)00041-1  
31

32  
33 Bell, P.S., Osler, J.C., 2011. Mapping bathymetry using X-band marine radar data recorded from a  
34 moving vessel. *Ocean Dynamics*. 61, 2141–2156.  
35 DOI: 10.1007/s10236-011-0478-4  
36

37 Bell, P.S., Inventor; Natural Environment Research Council, assignee. 2014, march 3<sup>rd</sup>. Inter-tidal  
38 mapping. International Patent Application No. PCT/GB2014/050908.  
39

40 Coakley, D. B., Haldeman, P. M., Morgan, D. G., Nicolas, K. R., Penndorf, D. R., Wetzell, L. B., & Weller,  
41 C. S. 2001. Electromagnetic scattering from large steady breaking waves. *Experiments in fluids*, 30(5),  
42 479-487.  
43 DOI: 10.1007/s003480000220  
44

45  
46 Dankert, H., Horstmann, J., 2007. A marine-radar wind sensor. *J. Atmos. Ocean. Technol.* 34(3),  
47 1629-1642.  
48 DOI: 10.1175/JTECH2083.1  
49

50  
51 Davidson, M., Van Koningsveld, M., de Kruif, A., Rawson, J., Holman, R., Lamberti, A., Medina, R.,  
52 Kroon, A., Aarninkhof, S., 2007. The CoastView project: Developing video-derived Coastal State  
53 Indicators in support of coastal zone management. *Coastal Engineering*. 54 (6-7), 463-475.  
54 DOI: 10.1016/j.coastaleng.2007.01.007  
55

56  
57 De Vriend, H.J., Wang, Z.B., Ysebaert, T., Herman, P.M.J., Ding, P., 2011. Eco-Morphological Problems  
58 in the Yangtze Estuary and the Western Scheldt. *Wetlands* 31, 1033–1042.  
59 DOI: 10.1007/s13157-011-0239-7  
60  
61  
62  
63  
64  
65

1  
2  
3  
4 Diop, S., Barousseau, J.-P., Descamps, C., 2014. The Land/Ocean Interaction in the Coastal Zone of  
5 West and Central Africa. Springer, New York.  
6 DOI 10.1007/978-3-319-06388-1  
7

8  
9 Fernandes, R., Vinzon, S., Oliveira, F. de, 2007. Navigation at the Amazon River Mouth: sand bank  
10 migration and depth surveying. Ports.  
11 DOI: [10.1061/40834\(238\)52](https://doi.org/10.1061/40834(238)52)  
12

13 Fisher, J.S., Stauble, D.K., 1977. Impact of Hurricane Belle on Assateague Island washover. *Geology*.  
14 5(12), 765–768.  
15 DOI: [10.1130/0091-7613\(1977\)5<765:IOHBOA>2.0.CO;2](https://doi.org/10.1130/0091-7613(1977)5<765:IOHBOA>2.0.CO;2)  
16

17  
18 FitzGerald, D., Kraus, N., Hands, E., 2000. Natural mechanisms of sediment bypassing at tidal inlets.  
19 U.S. Army Corps of Engineers. Coastal Engineering Technical Note CHETN-IV-30. U.S. Army Engineer  
20 Research and Development Center, Coastal and Hydraulics Laboratory. Vicksburg, MS. 1-10.  
21

22  
23 Fitzgerald, D.M., Heteren, S. Van, Montello, T.M., 1994. Shoreline Processes and Damage Resulting  
24 from the Halloween Eve Storm of 1991 along the North and South Shores of Massachusetts Bay,  
25 U.S.A. *J. Coast. Res.* 10(1), 113–132.  
26

27  
28 Flampouris, S., Seemann, J., Ziemer, F., 2009 Sharing our experience using wave theories inversion  
29 for the determination of the local depth. In: OCEANS. 2009-Europe Bremen.  
30 DOI: [10.1109/OCEANSE.2009.5278331](https://doi.org/10.1109/OCEANSE.2009.5278331)  
31

32  
33 Fuchs, J., Regas, D., Waseda, T., Welch, S., & Tulin, M. P. 1999. Correlation of hydrodynamic features  
34 with LGA radar backscatter from breaking waves. *Geoscience and Remote Sensing, IEEE Transactions*  
35 *on*, 37(5), 2442-2460.  
36 DOI:[10.1109/36.789641](https://doi.org/10.1109/36.789641)  
37

38  
39 Gao, J., 2009. Bathymetric mapping by means of remote sensing: methods, accuracy and limitations.  
40 *Progress in Physical Geography.* 33(1), 103–116.  
41 DOI: [10.1177/0309133309105657](https://doi.org/10.1177/0309133309105657)  
42

43  
44 Garcia D, 2010, Robust smoothing of gridded data in one and higher dimensions with missing values.  
45 *Computational Statistics & Data Analysis*, 54 : 1167-1178. DOI: [10.1016/j.csda.2009.09.020](https://doi.org/10.1016/j.csda.2009.09.020)

46  
47 Gaudin, D., Delacourt, C., Allemand, P., Jaud, M., Ammann, J., Tisseau, C., & Cuq, V. 2009. High  
48 resolution DEM derived from thermal infrared images: example of Aber Benoit (France).  
49 In *Geoscience and Remote Sensing Symposium, 2009 IEEE International, IGARSS 2009* (Vol. 4, pp. IV-  
50 705). IEEE.  
51 DOI: [10.1109/IGARSS.2009.5417474](https://doi.org/10.1109/IGARSS.2009.5417474)  
52

53  
54 Guenther, G.C., Brooks, M.W., LaRocque, P.E., 2000. New capabilities of the “SHOALS” airborne  
55 LiDAR bathymeter. *Remote Sensing of Environment.* 73(2) 247-255.  
56 DOI: [10.1016/S0034-4257\(00\)00099-7](https://doi.org/10.1016/S0034-4257(00)00099-7)  
57

58  
59 Hessner, K., Bell, P.S., 2009. High resolution current & bathymetry determined by nautical X-Band  
60 radar in shallow waters. In: OCEANS. 2009-Europe Bremen.  
61 DOI: [10.1109/OCEANSE.2009.5278333](https://doi.org/10.1109/OCEANSE.2009.5278333)  
62  
63  
64  
65

1  
2  
3  
4 Hessner, K., Reichert, K., Rosenthal, W., 1999. Mapping of sea bottom topography in shallow seas by  
5 using a nautical radar. In: 2nd Symposium on Operationalization of Remote Sensing Enschede, The  
6 Netherlands, 16-20 August, 1999.

7  
8 Hessner, K., Reichert, K., Borge, J. C. N., Stevens, C. L., & Smith, M. J. (2014). High-resolution X-Band  
9 radar measurements of currents, bathymetry and sea state in highly inhomogeneous coastal  
10 areas. *Ocean Dynamics*, 64(7), 989-998.

11  
12  
13 Heygster, G., Dannenberg, J., Notholt, J., 2010. Topographic Mapping of the German Tidal Flats  
14 Analyzing SAR Images With the Waterline Method. *IEEE Trans. Geosci. Remote Sens.* 48(3), 1019–  
15 1030.

16  
17 DOI: 10.1109/TGRS.2009.2031843

18  
19 Holland, K.T., Holman, R.A., Lippmann, T.C., Stanley, J., Member, A., Plant, N., 1997. Practical Use of  
20 Video Imagery in Nearshore Oceanographic Field Studies. *IEEE Journal of Oceanic Engineering.* 22(1),  
21 81–92.

22  
23 DOI: 10.1109/48.557542

24  
25 Holman, R. A., Bowen, A. J., 1979. Edge waves on complex beach profiles. *J. Geophys. Res.* 84(C10),  
26 6339-6346.

27  
28 DOI: 10.1029/JC084iC10p06339

29  
30 Holman, R. A., Stanley, J., 2007. The history and technical capabilities of Argus. *Coastal Engineering*  
31 54(6-7), 477–491.

32  
33 DOI: 10.1016/j.coastaleng.2007.01.003

34  
35 Holman, R., Sallenger, A., Lippmann, T., Haines, J., 1993. The Application of Video Image Processing  
36 to the Study of Nearshore Processes. *Oceanography.* 6(3), 78–85.

37  
38 DOI:10.5670/oceanog.1993.02

39  
40 Holman, R., Haller, M.C., 2013. Remote sensing of the nearshore. *Ann. Rev. Mar. Sci.* 5, 95–113.

41  
42 DOI: 10.1146/annurev-marine-121211-172408

43  
44 Ja, S. J., West, J. C., Qiao, H., & Duncan, J. H. 2001. Mechanisms of low-grazing-angle scattering from  
45 spilling breaker water waves. *Radio Science*,36(5), 981-998.

46  
47 Koopmans, B.N., Wang, Y., 1994. Satellite radar data for topographic mapping of the tidal flats in the  
48 Wadden Sea, The Netherlands. In: *Proceedings of the Second Thematic Conference on Remote*  
49 *Sensing for Marine and Coastal Environments, New Orleans. Vol 31.*

50  
51 Liu, Y., Li, M., Mao, L., Cheng, L., Chen, K., 2013. Seasonal Pattern of Tidal-Flat Topography along the  
52 Jiangsu Middle Coast, China, Using HJ-1 Optical Images. *Wetlands* 33(5).

53  
54 DOI:10.1007/s13157-013-0445-6

55  
56 Lynch, P.J., Wagner, R.J., 1970. Rough-Surface Scattering: Shadowing, Multiple Scatter, and Energy  
57 Conservation. *J. Math. Phys.* 11(10), 3032.

58  
59 DOI: 10.1063/1.1665090

60  
61  
62  
63  
64  
65

1  
2  
3  
4 Lyzenga, D. R. 1985. Shallow-water bathymetry using combined LiDAR and passive multispectral  
5 scanner data. *International Journal of Remote Sensing*,6(1), 115-125.

6 DOI: [10.1109/36.992783](https://doi.org/10.1109/36.992783)  
7

8 Mason, D.C., Davenport, I., Robinson, G.J., Flather, R.A., McCartney, B.S., 1995. Construction of an  
9 inter-tidal digital elevation model by the "Water-line"Method. *Geophysical Research Letters*. 22(23),  
10 3187–3190.

11 DOI: [10.1029/95GL03168](https://doi.org/10.1029/95GL03168)  
12

13  
14 Mason, D.C., Garg, P.K., 2001. Morphodynamic Modelling of Intertidal Sediment Transport in  
15 Morecambe Bay. *Estuar. Coast. Shelf Sci.* 53(1), 79–92.

16 DOI:10.1006/ecss.2000.0618  
17

18  
19 Mason, D.C., Amin, M., Davenport, I.J., Flather, R. A., Robinson, G.J., Smith, J. A., 1999. Measurement  
20 of Recent Intertidal Sediment Transport in Morecambe Bay using the Waterline Method. *Estuar.*  
21 *Coast. Shelf Sci.* 49(3), 427–456.

22 DOI: [10.1006/ecss.1999.0508](https://doi.org/10.1006/ecss.1999.0508)  
23

24  
25 Mattie, M., Harris, D., 1978. The use of imaging radar in studying ocean waves. *Coastal Engineering*  
26 *Proceedings*. 1(16). 174–189.

27 DOI: [10.9753/icce.v16](https://doi.org/10.9753/icce.v16).  
28

29  
30 McCann, D.L., 2007, Dune tracking in the Dee with X-band radar: a new remote sensing technique  
31 for quantifying bedload transport. MSc thesis, Bangor University.  
32

33  
34 McCann, D.L. & Bell, P.S. 2014 Marine Radar Derived Current Vector Mapping at a Planned  
35 Commercial Tidal Stream Turbine Array in the Pentland Firth, U.K. MTS/IEEE Oceans 2014  
36 Conference, St Johns, Newfoundland, Canada, 14-19 September 2014.  
37

38  
39 Moore, R.D., Wolf, J., Souza, A.J., Flint, S.S., 2009. Morphological evolution of the Dee Estuary,  
40 Eastern Irish Sea, UK: A tidal asymmetry approach. *Geomorphology*. 103, 588–596.

41 DOI: [10.1016/j.geomorph.2008.08.003](https://doi.org/10.1016/j.geomorph.2008.08.003)  
42

43  
44 Morton, A., Gibeaut, J.C., Paine, J.G., 1995. Meso-scale transfer of sand during and after storms:  
45 implications for prediction of shoreline movement. *Marine Geology*. 126, 161–179.

46 DOI: [10.1016/0025-3227\(95\)00071-6](https://doi.org/10.1016/0025-3227(95)00071-6)  
47

48  
49 Nicholls, R.L., Marston, A.F., 1939. Shoreline changes in Rhode Island produced by Hurricane of  
50 September 21, 1938. *Bull. Geol. Soc. Am.* 50(9), 1357–1370.

51 DOI: [10.1130/GSAB-50-1357](https://doi.org/10.1130/GSAB-50-1357)  
52

53  
54 Nieto Borge, J.C., Rodríguez, G.R., Hessner, K., González, P.I., 2004. Inversion of Marine Radar Images  
55 for Surface Wave Analysis. *J. Atmos. Ocean. Technol.* 21(8), 1291–1300.

56 DOI: [http://dx.doi.org/10.1175/1520-0426\(2004\)021<1291:IOMRIF>2.0.CO;2](http://dx.doi.org/10.1175/1520-0426(2004)021<1291:IOMRIF>2.0.CO;2)  
57

58  
59 Nieto Borge, J.C., Guedes Soares, C., 2000. Analysis of directional wave fields using X-band  
60 navigation radar. *Coast. Eng.* 40(4), 375–391.

61 DOI: [10.1016/S0378-3839\(00\)00019-3](https://doi.org/10.1016/S0378-3839(00)00019-3)  
62  
63  
64  
65

1  
2  
3  
4 Nieto Borge, J.C., Hessner, K., Jarabo-Amores, P., de la Mata-Moya, D., 2008. Signal-to-noise ratio  
5 analysis to estimate ocean wave heights from X-band marine radar image time series. IET Radar  
6 Sonar Navig. 2(1), 35–41.  
7 DOI: 10.1049/iet-rsn  
8

9  
10 Plant, N.G., Holman, R. A., 1997. Intertidal beach profile estimation using video images. Mar. Geol.  
11 140(1-2), 1–24.  
12 DOI: 10.1016/S0025-3227(97)00019-4  
13

14 Reichert, K., Hessner, K., Nieto Borge, J.C., Dittmer, J., 1999. WaMoS II: a radar based wave and  
15 current monitoring system. In: Proceedings of ISOPE 1999, Brest. 3, 1–5.  
16

17 Richards, M.A., 2005. Fundamentals of radar signal processing. McGraw-Hill Education, India.  
18

19 Rosati, J.D., Kraus, N.C., 2000. "Shoal-Reduction strategies for entrance channels" Coastal  
20 Engineering Technical Note CETN-IV-22. U.S. Army Engineer Research and Development Center,  
21 Coastal and Hydraulics Laboratory. Vicksburg, MS.  
22

23  
24 Ryu, J.-H., Won, J.-S., Min, K.-D., 2002. Waterline extraction from Landsat TM data in a tidal flat A  
25 case study in Gomso Bay , Korea. Remote Sensing of Environment. 83, 442–456.  
26 DOI: 10.1016/S0034-4257(02)00059-7  
27

28  
29 Ryu, J.-H., Kim, C.-H., Lee, Y.-K., Won, J.-S., Chun, S.-S., Lee, S., 2008. Detecting the intertidal  
30 morphologic change using satellite data. Estuar. Coast. Shelf Sci. 78(4), 623–632.  
31 DOI: 10.1016/j.ecss.2008.01.020  
32

33  
34 Santiago, I. De, Morichon, D., Abadie, S., Castelle, B., Liria, P., Epelde, I., 2013. Video monitoring  
35 nearshore sandbar morphodynamics on a partially engineered embayed beach. Journal of Coastal  
36 Research Special Issue 65. 458–463.  
37 DOI: 10.2112/SI65-078.1  
38

39  
40 Senet, C.M., Seemann, J., Flampouris, S., Ziemer, F., 2008. Determination of Bathymetric and Current  
41 Maps by the Method DiSC Based on the Analysis of Nautical X-Band Radar Image Sequences of the  
42 Sea Surface (November 2007). IEEE Trans. Geosci. Remote Sens. 46(8), 2267–2279.  
43 DOI: 10.1109/TGRS.2008.916474  
44

45  
46 Serafino, F., Lugni, C., Soldovieri, F., 2010. A Novel Strategy for the Surface Current Determination  
47 From Marine X-Band Radar Data. IEEE Geosci. Remote Sens. Lett. 7(2), 231–235.  
48 DOI: 10.1109/LGRS.2009.2031878  
49

50  
51 Sexton, W. j., Moslow, T.F., 1981. Effects on Hurricane David 1979. on the beaches of Seabrook  
52 Island South Carolina. Northeast. Geol. 3, 297–305.  
53

54 Stive, M.J.F., de Schipper, M.A., Luijendijk, A.P., Aarninkhof, S.G.J., van-Gelder-Maas, C., van Thiel de  
55 Vries, J.S.M., de Vries, S., Henriquez, M., Marx, S., Ranasinghe, R., 2013. A New Alternative to Saving  
56 Our Beaches from Sea-Level Rise: The Sand Engine. Journal of Coastal Research. 29(5),1001-1008.  
57  
58  
59  
60  
61  
62  
63  
64  
65

- 1  
2  
3  
4 Sobral, F., Pereira, P., Cavalcanti, P., Guedes, R., Calliari, L., 2013. Intertidal Bathymetry Estimation  
5 Using Video Images on a Dissipative Beach. *Journal of Coastal Research Special issue* 65. 1439–1444.  
6 DOI: 10.2112/SI65-243.1  
7
- 8 Stone, G.W., Grymes, J.M., Armbruster, C.K., Xu, J.P., Huh, O.K., 1996. Researchers Study Impact of  
9 Hurricane Opal on Florida Coast. *EOS, Trans. Am. Geophys. Un.* 77(19), 181–188.  
10
- 11 Takewaka, S. 2005. Measurements of shoreline positions and intertidal foreshore slopes with X-band  
12 marine radar. *Coastal Engineering Journal*, Vol. 47, Nos. 2 & 3 (2005) 91-107  
13
- 14 Trizna, D. B., Hansen, J. P., Hwang, P., & Wu, J. 1991. Laboratory studies of radar sea spikes at low  
15 grazing angles. *Journal of Geophysical Research: Oceans* (1978–2012), 96(C7), 12529-12537.  
16
- 17 Uunk, L., Wijnberg, K. M., & Morelissen, R. 2010. Automated mapping of the intertidal beach  
18 bathymetry from video images. *Coastal engineering*, 57(4), 461-469.  
19 DOI:10.1016/j.coastaleng.2009.12.002  
20
- 21 Valenzuela, G., 1978. Theories for the interaction of electromagnetic and oceanic waves—A review.  
22 *Boundary-Layer Meteorology*. 13, 61–85.  
23 DOI: 10.1007/BF00913863  
24
- 25 van der Wal, D., Forster, R. M., Rossi, F., Hummel, H., Ysebaert, T., Roose, F., & Herman, P. M. 2011.  
26 Ecological evaluation of an experimental beneficial use scheme for dredged sediment disposal in  
27 shallow tidal waters. *Marine pollution bulletin*, 62(1), 99-108.  
28 DOI: 10.1016/j.marpolbul.2010.09.005  
29
- 30 Way, O., 2013, The migration of large scale bed forms in the Dee Estuary. PhD Thesis, University of  
31 Bangor, Wales.  
32
- 33 Wolf, J., Brown, J.M., Howarth, M.J., 2011. The wave climate of Liverpool Bay—observations and  
34 modelling. *Ocean Dynamics*. 6(5), 639–655.  
35 DOI: 10.1007/s10236-011-0376-9  
36
- 37 Yoder, N. (2011). PeakFinder(Matlab program). *Internet: [http://www.mathworks.com-](http://www.mathworks.com/matlabcentral/fileexchange/25500)*  
38 */matlabcentral/fileexchange/25500.*  
39
- 40 Young, I.R., Rosenthal, W., Ziemer, F., 1985. A Three-Dimensional Analysis of Marine Radar Images  
41 for the Determination of Ocean Wave Directionality and Surface Currents. *J. Geophys. Res.* 90(C1),  
42 1049–1059.  
43 DOI: 10.1029/JC090iC01p01049  
44  
45  
46  
47  
48  
49  
50  
51  
52  
53  
54  
55  
56  
57  
58  
59  
60  
61  
62  
63  
64  
65

1  
2  
3  
4  
5  
6 *Figure 1: A photo of the radar tower looking north on Hilbre Island.*

7  
8 *Figure 2: Study area showing key points in the Dee Estuary with radar location and range.*

9  
10 *Figure 3: Snapshot radar image from Hilbre Island showing high returns from the coastline and*  
11 *breaking waves along the waterline.*

12  
13 *Figure 4: Time exposure radar image representing ten minutes of data showing general patterns of*  
14 *wave breaking and sea clutter.*

15  
16 *Figure 5: (a) The Hilbre Island tide gauge data from September 2006 to summer 2009. The region*  
17 *plotted in blue relates to the present study period; (b) The Hilbre Island tidal residual calculated with*  
18 *respect to a tidal prediction; (c) The class 'A' Liverpool Gladstone Dock Tide Gauge Residual; (d) The*  
19 *Hilbre Island synthetic tide constructed from the tidal prediction + the Gladstone Dock residual. The*  
20 *region plotted in blue represents the period spanning the present study; (e) The Hilbre Island residual*  
21 *with respect to the Hilbre Island synthetic tide.*

22  
23 *Figure 6: The tidal residuals (Measured minus predicted) for Hilbre Island compared with Liverpool*  
24 *Gladstone Dock showing a strong  $R^2$  of 0.9.*

25  
26 *Figure 7: A subsection of the tidal data for Hilbre Island, with the tide prediction marked as the red*  
27 *dotted line, the Hilbre tide gauge data which was considered valid during that period, marked in*  
28 *cyan, and the synthetic tide marked as the black dots. The highlighted grey area corresponds to the*  
29 *period during which the LiDAR survey was flown.*

30  
31 *Figure 8: Time-exposure image timestack used to form 3D matrix from which pixel intensities are*  
32 *extracted at each time step and location.*

33  
34 *Figure 9: (a) Tidal elevations over two weeks sampled concurrently with the radar time-exposure*  
35 *image; (b) Matrix of binary wet-dry values based on tidal elevation; (c) Example row extracted from b*  
36 *showing the tidal square wave indicating wet or dry at a water level of 5 m ACD; (d) Raw pixel*  
37 *intensities over two weeks extracted from a single location; (e) Absolute gradient of the tidal square*  
38 *wave showing transition times from wet to dry; (f) Processed gradient of the raw pixel time series,*  
39 *approximating the transition times from wet to dry at a given location.*

40  
41 *Figure 10: Correlation coefficients for a given pixel record at water levels within the tidal range.*

42  
43 *Figure 11: Maximum correlation values at every location across the survey area. The correlation*  
44 *coefficient at each point has been matched to a specific tidal water elevation above chart datum. The*  
45 *strength indicates the confidence of the derived elevation.*

46  
47 *Figure 12: Radar-derived elevations across the survey area showing beach profile and sandbanks in*  
48 *addition to the Hilbre channel and subtidal zone. Regions of interest include; (i) West Hoyle*  
49 *Sandbanks; (ii) The Welshman's Gut (ephemeral channel linking the two main channels of the Dee*  
50 *estuary); (iii) Hilbre Island; (iv) The Wirral Peninsula; (v) East Hoyle Bank; (vi) Hilbre Swash; (vii)*  
51 *Sandbank with wrecked vessel (see Figure 12).*

52  
53 *Figure 13: Location of the wrecked cargo ship SS Nestos. Photo courtesy of John M.X. Hughes.*  
54  
55  
56  
57  
58  
59  
60  
61  
62  
63  
64  
65

1  
2  
3  
4 *Figure 14: (a) The evolution of a radar backscatter cross-shore profile over ten minutes for the record*  
5 *starting 06:00 6<sup>th</sup> October 2006, with the wave breaker line clearly evident around x = 550 m. (b) The*  
6 *temporal mean of that backscatter profile (uncalibrated intensity scale). The cyan line marked on*  
7 *both plots indicates the location of the still water level with respect to the LiDAR survey in the middle*  
8 *(at 06:05 am) of the radar record. The red, green and blue lines mark the corresponding derived*  
9 *average waterlines from the two week period ending on the 8<sup>th</sup> October 2006 at the start, middle and*  
10 *end of the record respectively.*

11  
12  
13  
14 *Figure 15: Locations of cross-shore transects extracted and analysed over a ten month period.*

15  
16 *Figure 16: (a) Raw radar-derived elevations extracted along each cross-shore transect through time.*  
17 *Each row shows mean elevations over a two-week period; (b) Elevation transects from the same*  
18 *locations taken from data smoothed using a weighted linear filter; (c) Correlation coefficients at each*  
19 *point along extracted transects; (d) Differences between raw data and the filtered data, ensuring the*  
20 *introduction of smoothing artefacts is minimal.*

21  
22  
23 *Figure 17: Waterline Transects at the start (red) and end (blue) of the ten month study period. All*  
24 *transects show overall erosion and setback of the beach foreshore.*

25  
26 *Figure 18: Locations of rock control points and resulting elevations throughout the ten month*  
27 *analysis period, elevation records from the four sites, along with both raw (red) and smoothed (blue)*  
28 *elevations from each rock location.*

29  
30  
31 *Figure 19: Radar (a) and LiDAR (b) derived elevations during October 2006.*

32  
33 *Figure 20: Residuals between LiDAR and radar derived elevations.*

34  
35 *Figure 21: Elevations along each transect from Figure 15 with smoothed radar-derived (green) and*  
36 *LiDAR (blue) elevations.*

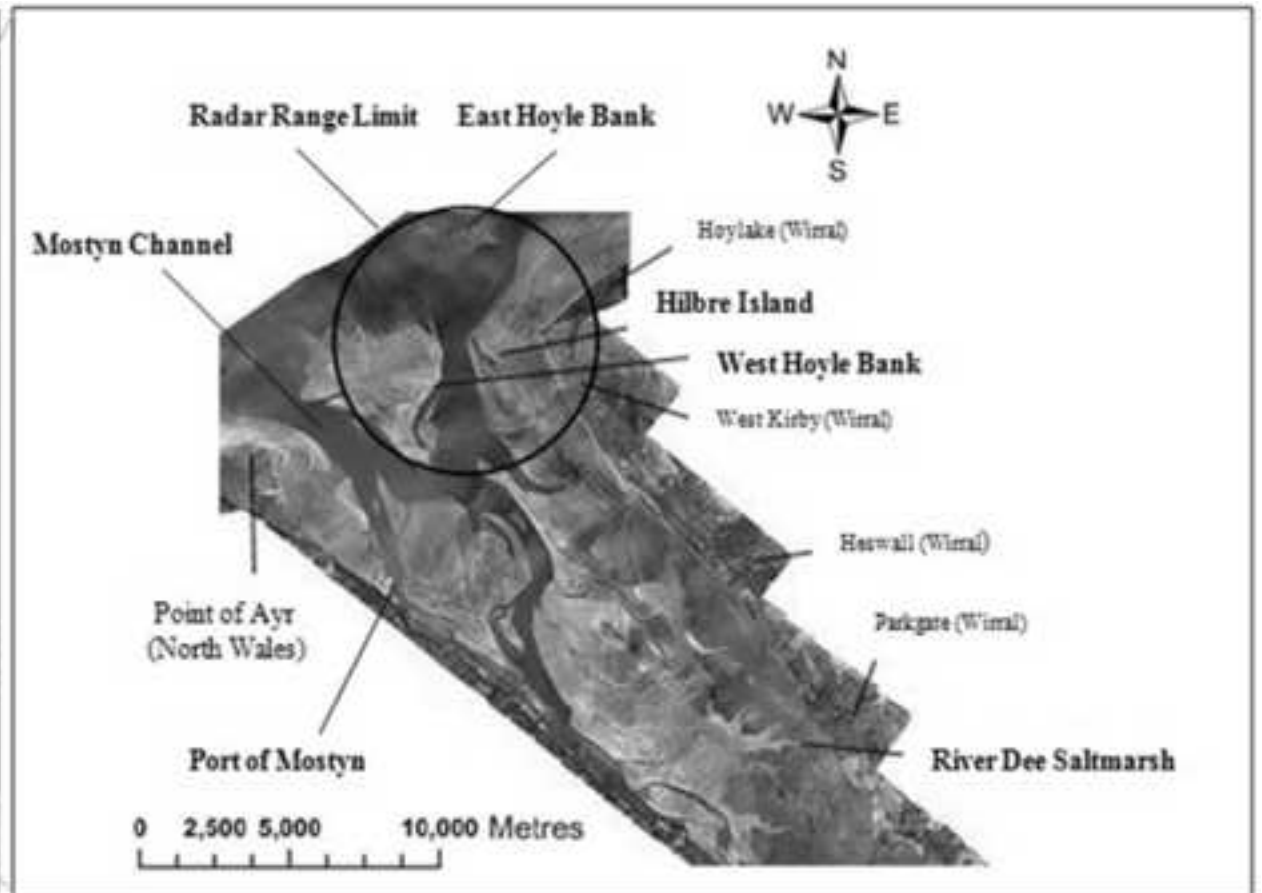
37  
38 *Figure 22: (a) Extracted subsection of radar-derived; (b) LiDAR elevations; (c) The residuals between*  
39 *radar-derived and LiDAR elevation data; (d) An artificial line of sight shadow map, illustrating the*  
40 *radar line of sight based on the LiDAR observations, constructed using a simple ray tracing algorithm.*

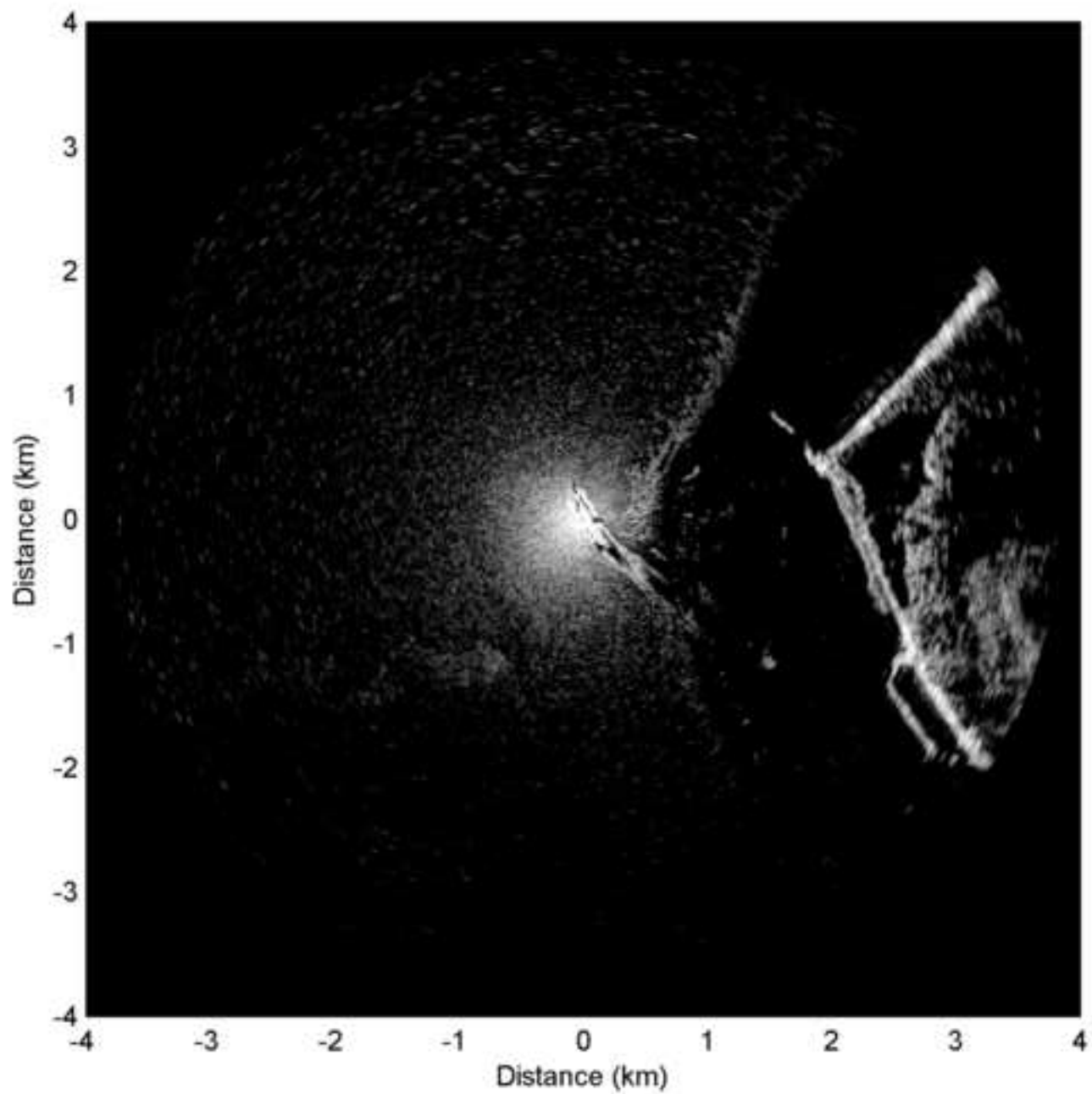
41  
42  
43 *Figure 23: Differences between the LiDAR and radar derived waterline elevations at different ranges*  
44 *from the radar (left) and corresponding error histograms (right): (a) the region within 0.75 km of the*  
45 *radar location; (b) the region from 0.75 km range to 1.5 km range; (c) the region from 1.5 km - 2.25*  
46 *km; (d) the region from 2.25 km – 3 km.*

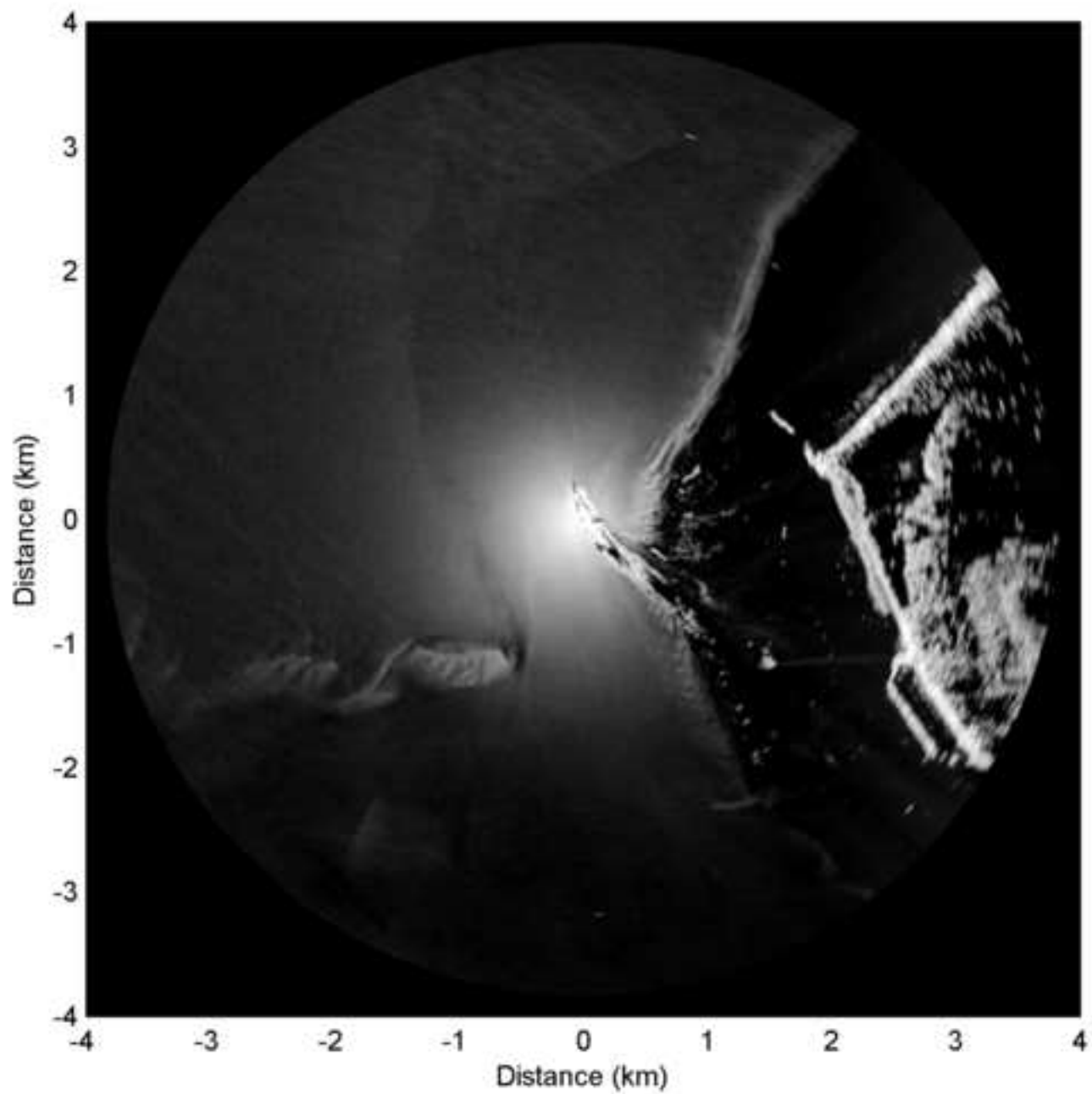
47  
48  
49 *Figure 24: Changes in waterline elevation from March 2006 to January 2007. Red indicates erosion*  
50 *while blue indicates accretion.*

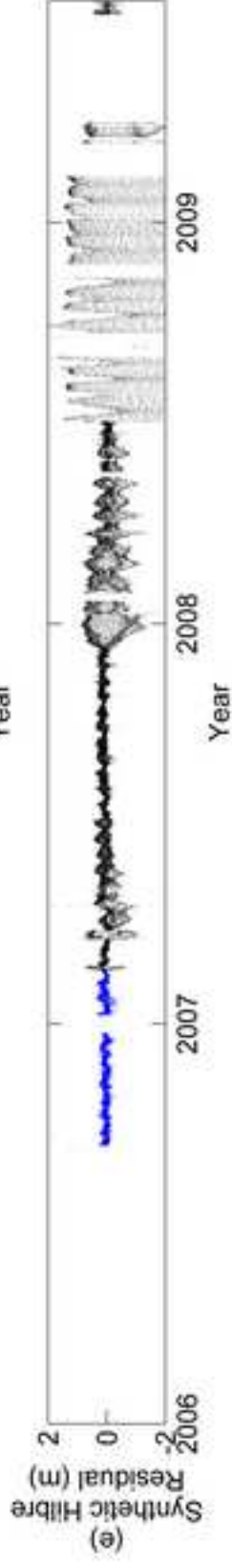
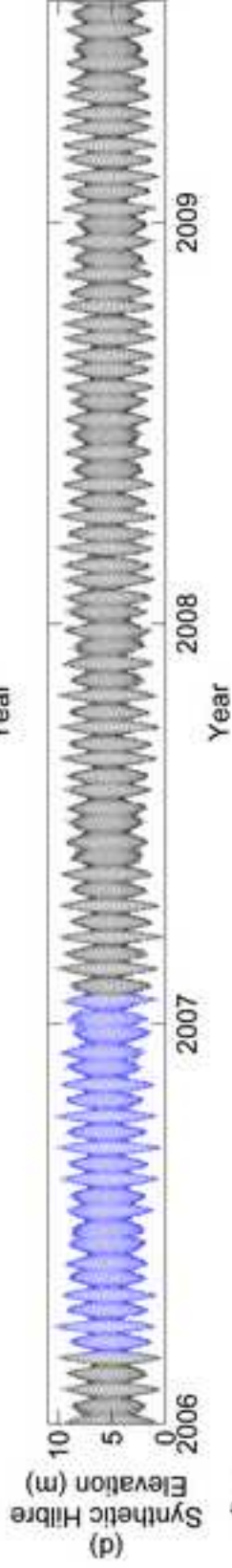
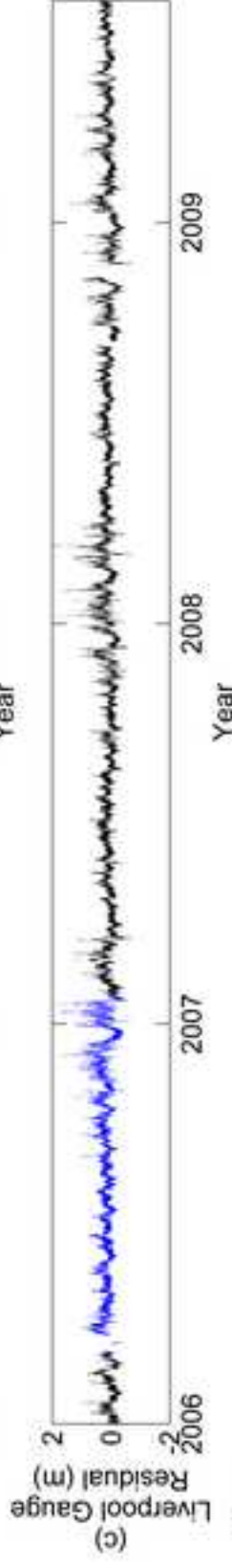
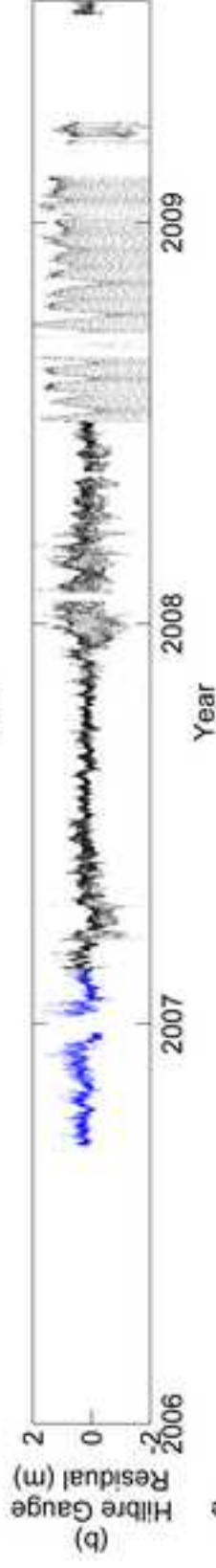
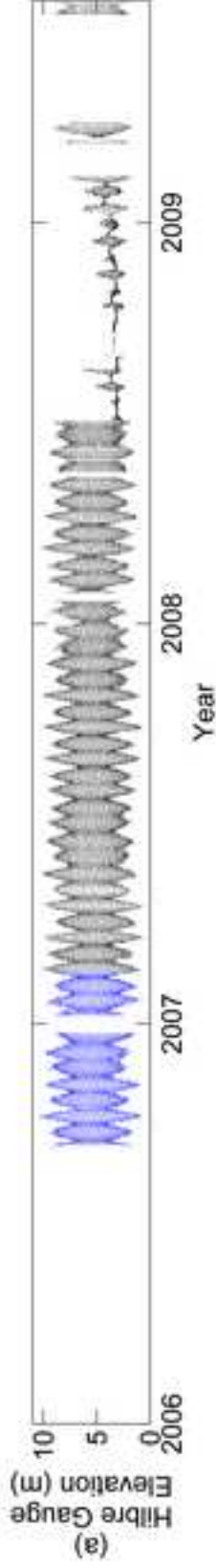
51  
52  
53  
54  
55  
56  
57  
58  
59  
60  
61  
62  
63  
64  
65

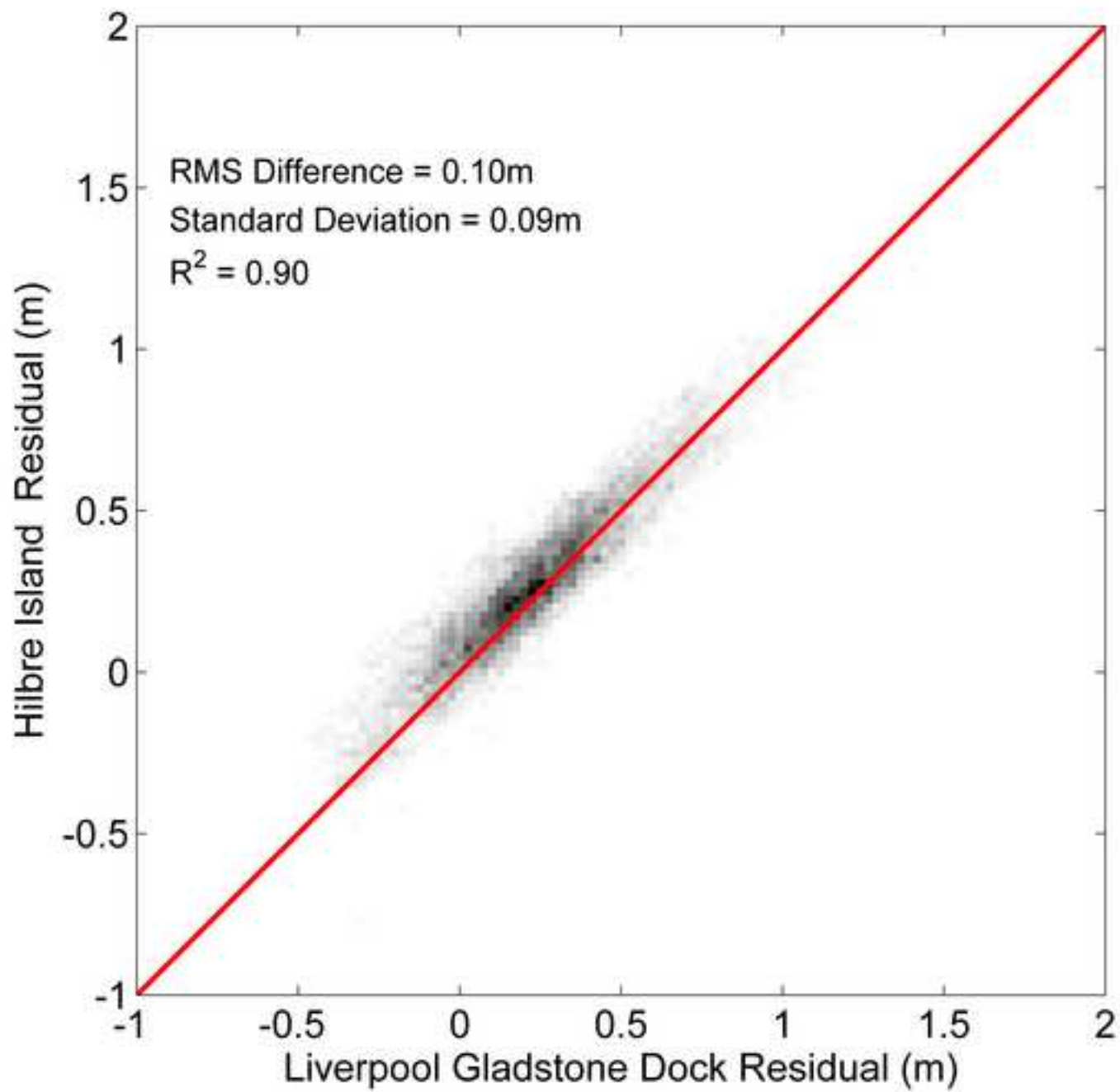


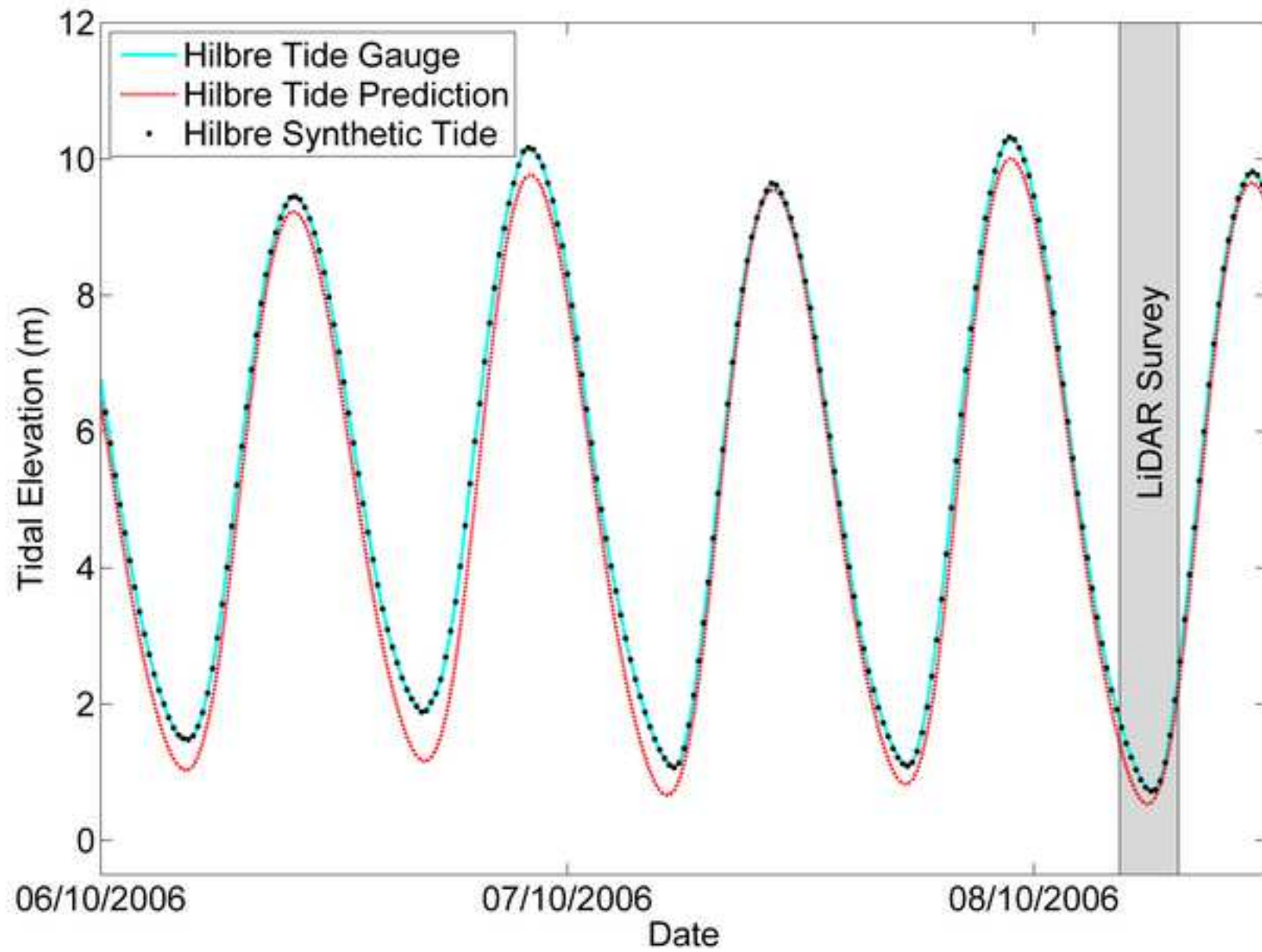


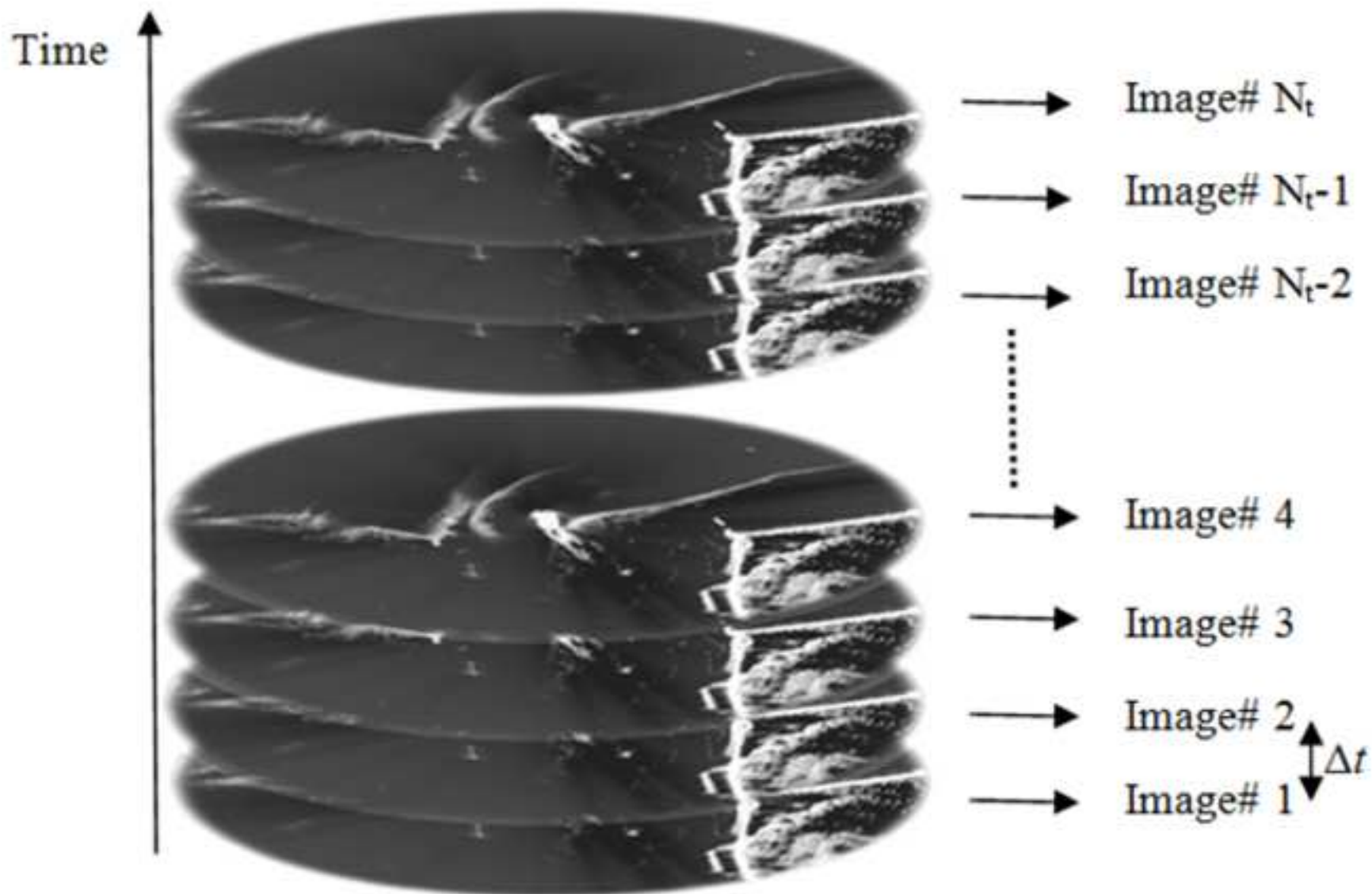


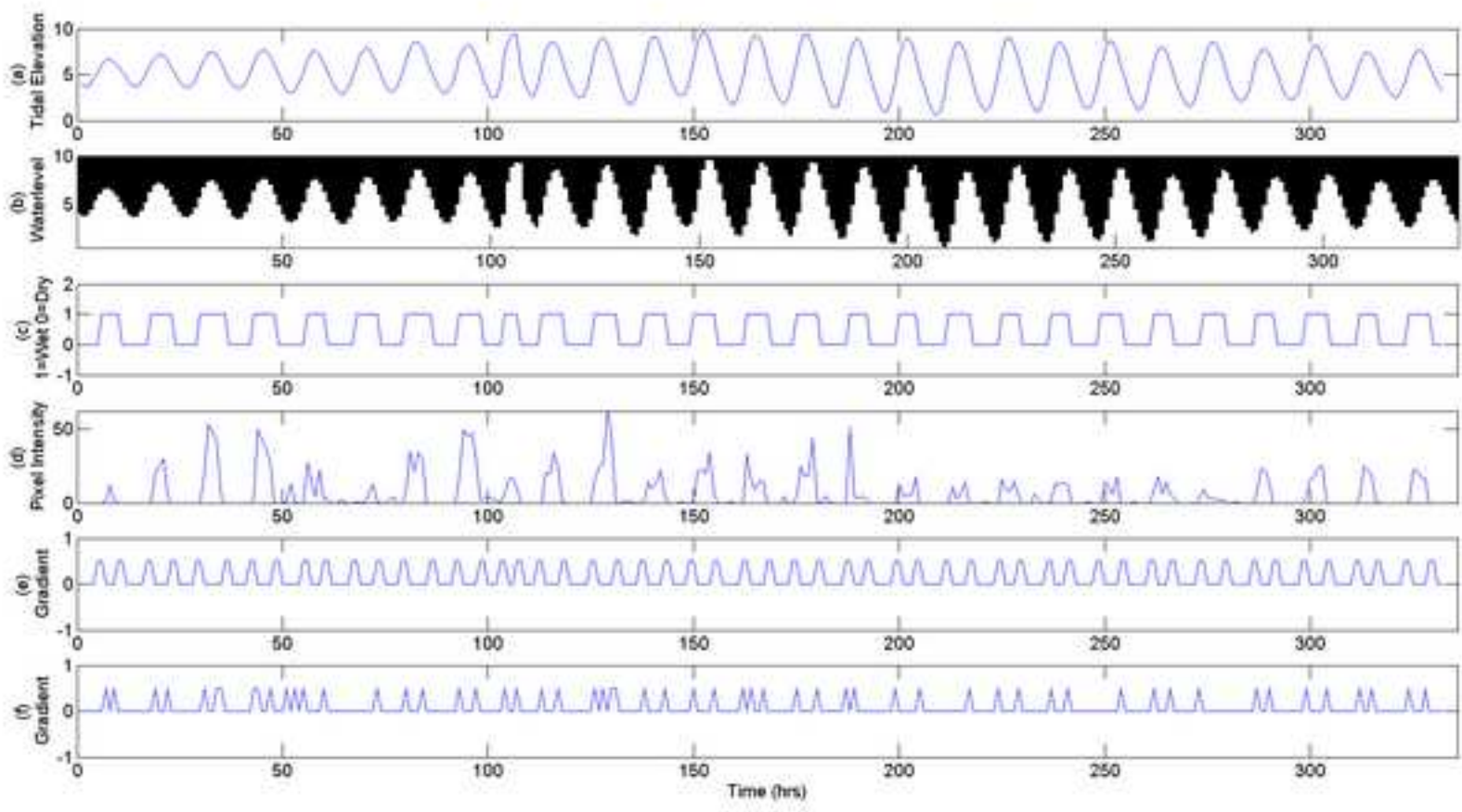


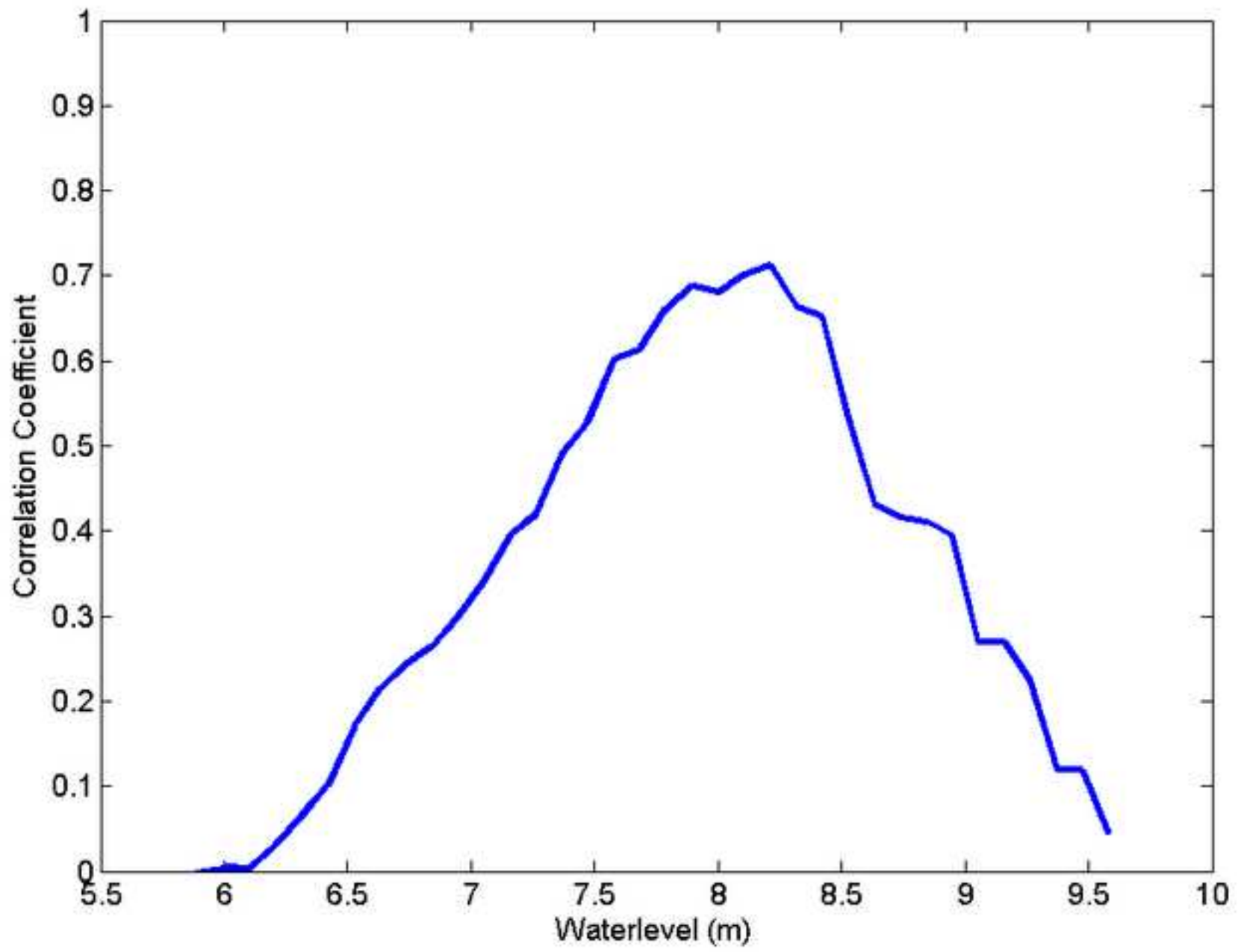


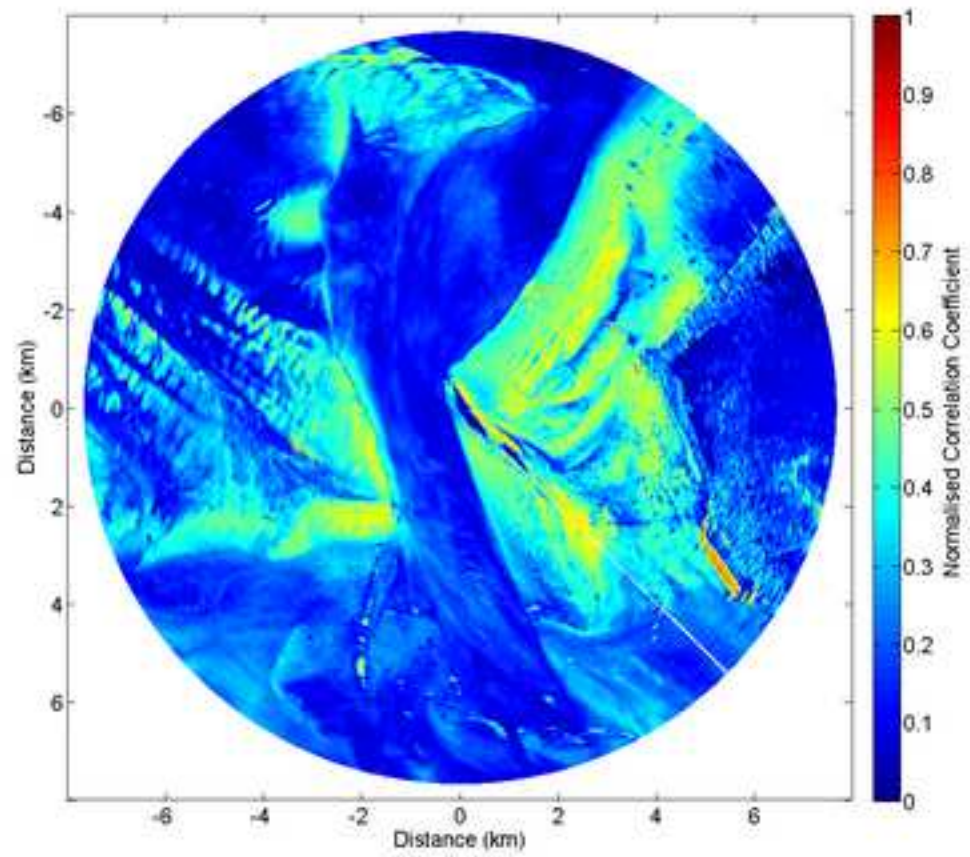


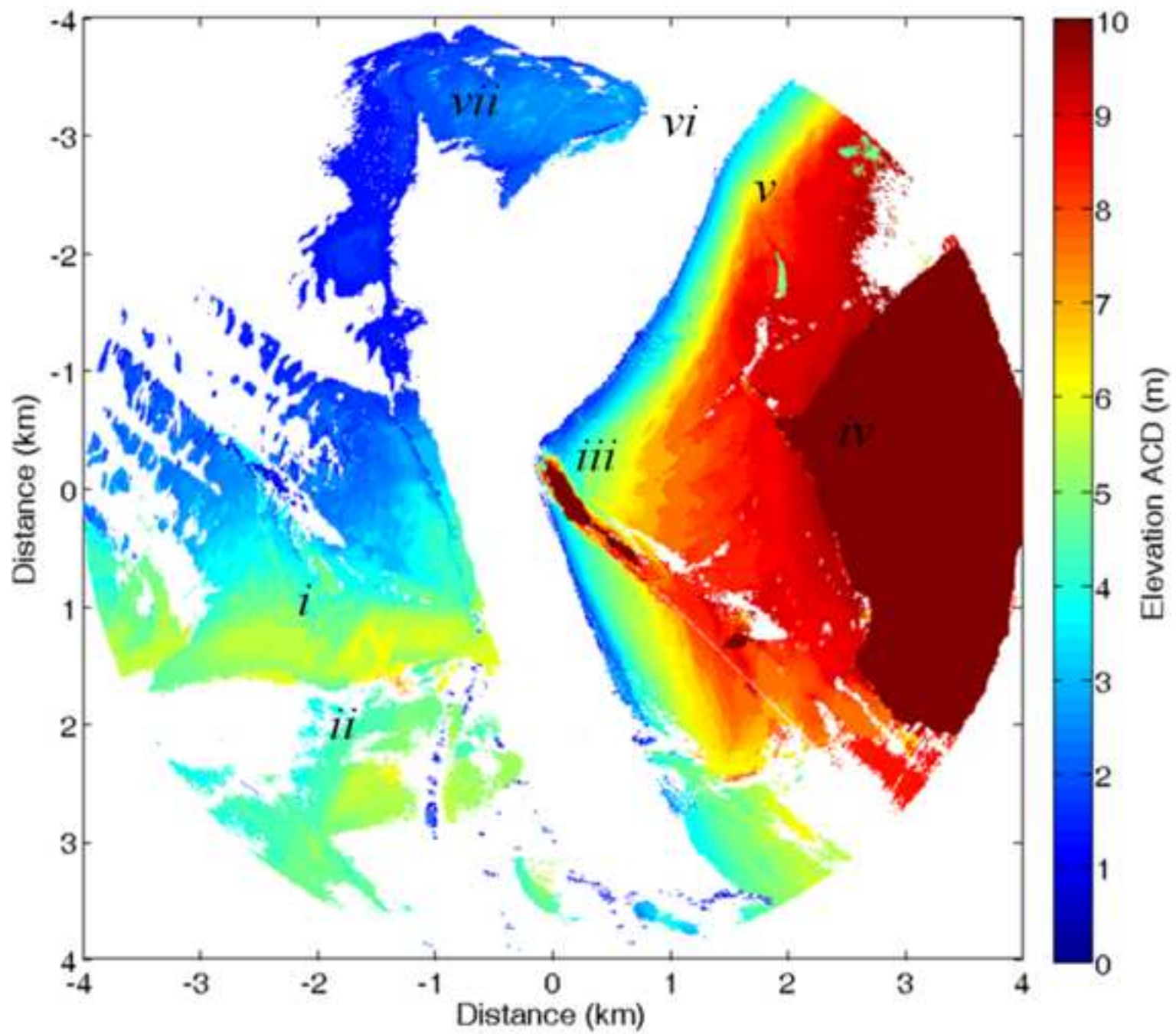


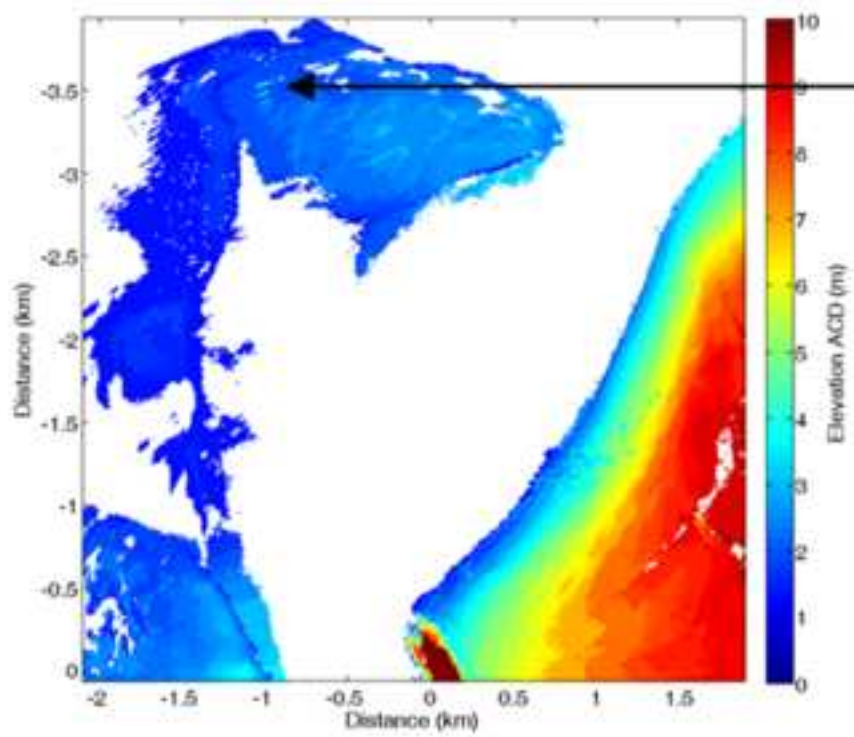


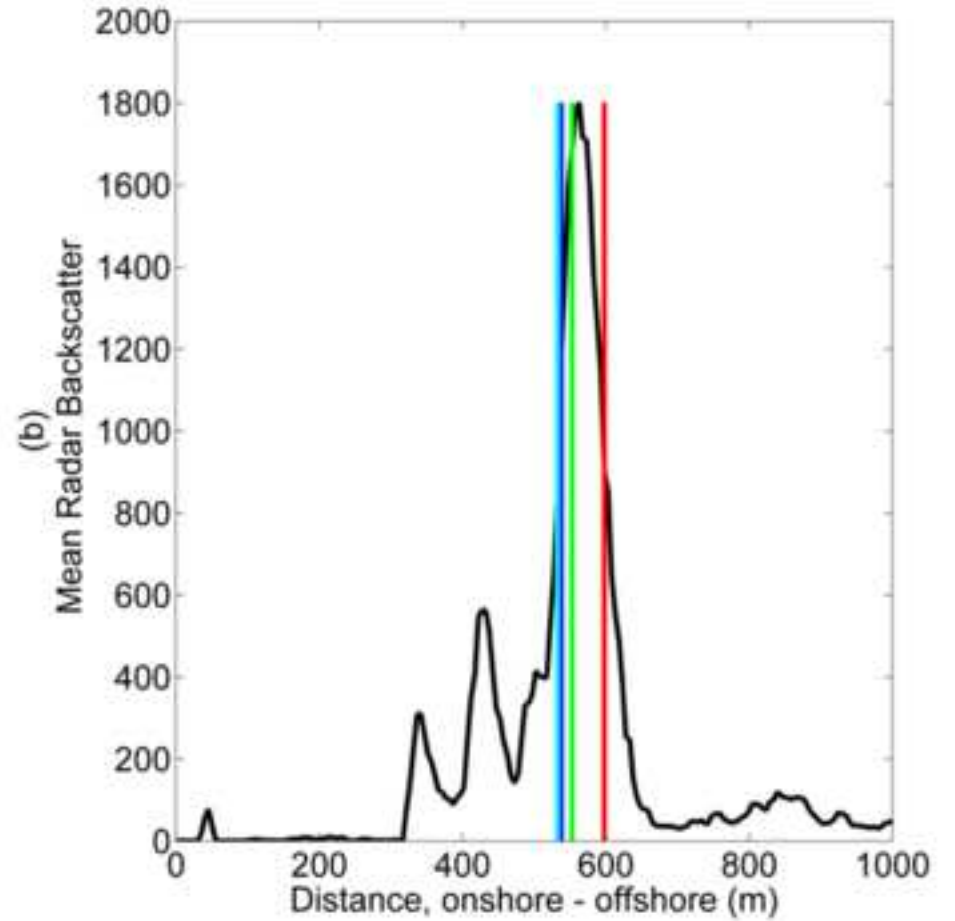
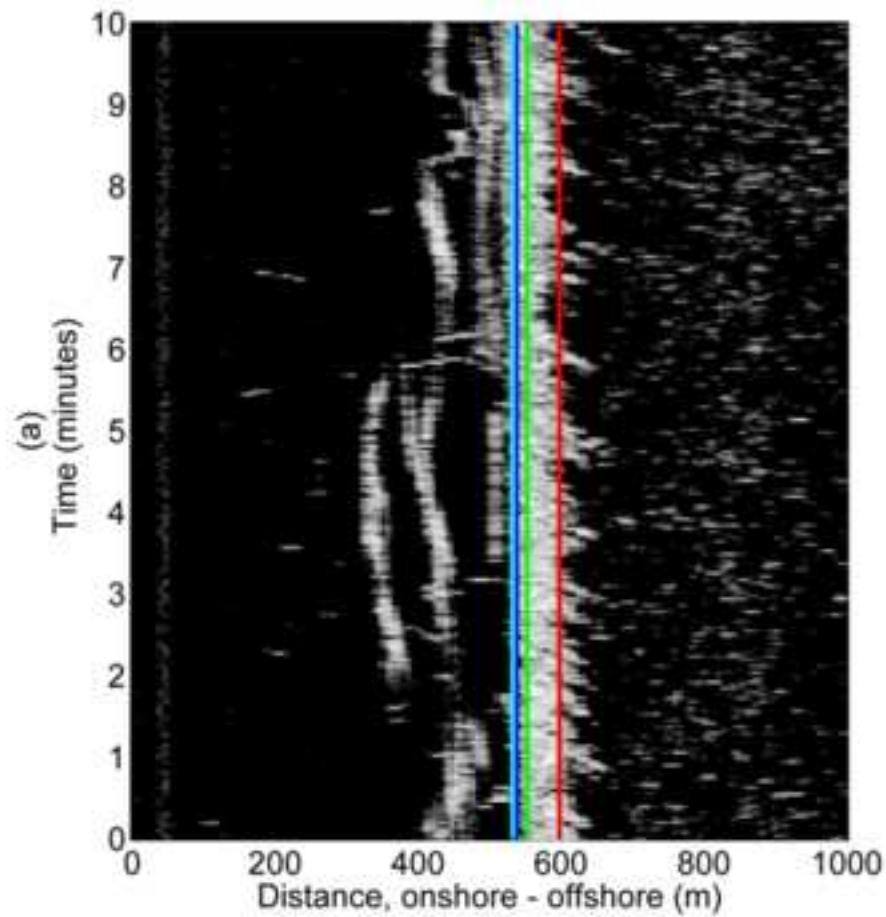




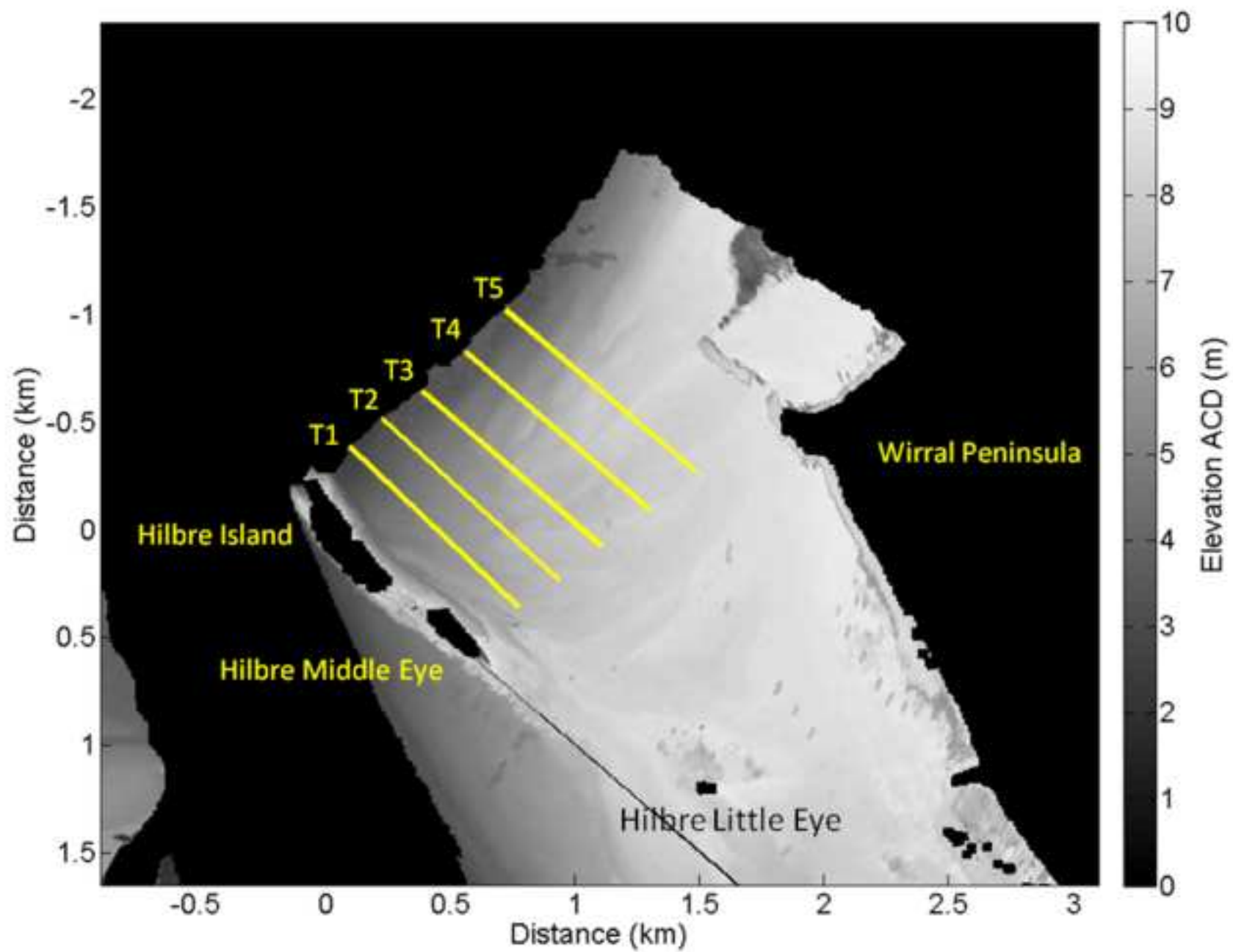


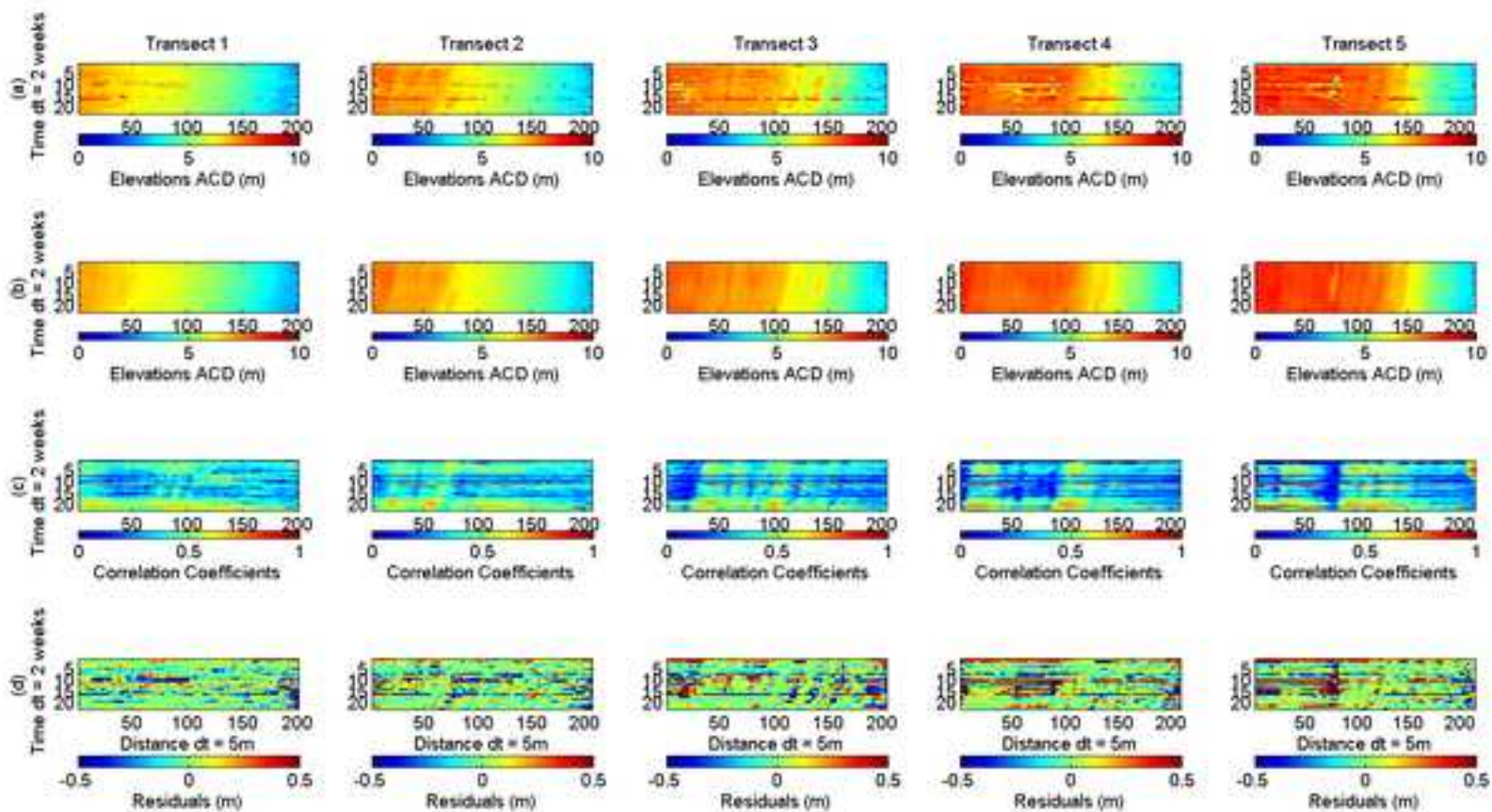


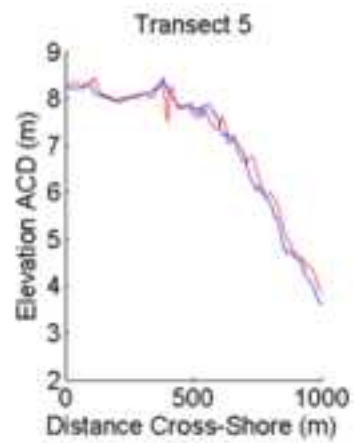
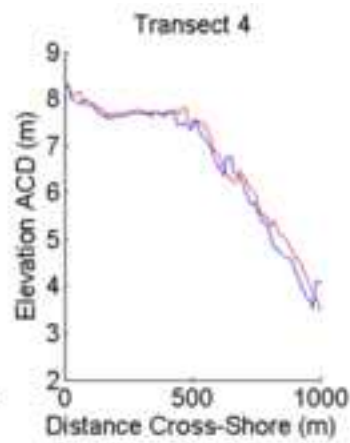
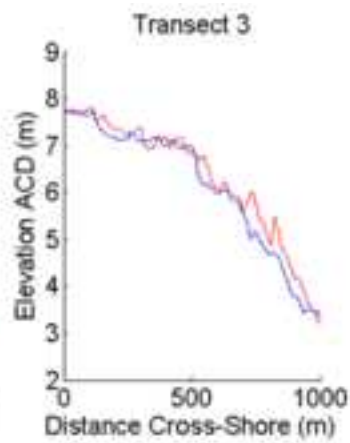
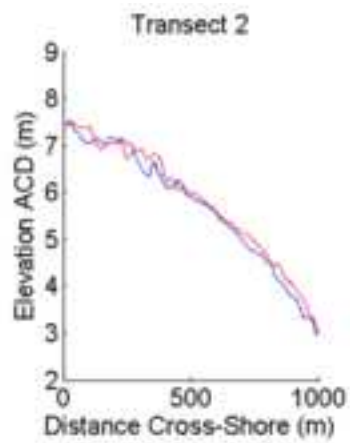
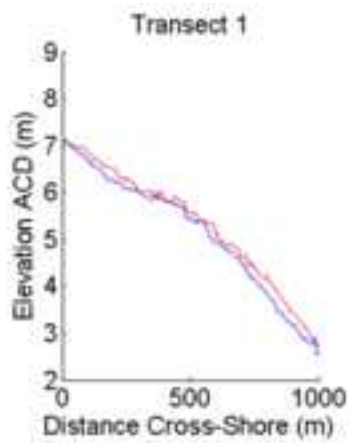




- Waterline elevation at 6.00am Tide=2.97 m
- Waterline elevation at 6.05am Tide=3.11 m
- Waterline elevation at 6.10am Tide=3.29 m
- LIDAR derived elevation = 3.11 m







Transect Elevations March 2006  
Transect Elevations January 2007

